Published in "Physical Review B 87(12): 125149, 2013"
which should be cited to refer to this work.

Screening and nonlocal correlations in the extended Hubbard model from self-consistent combined GW and dynamical mean field theory

Thomas Ayral,[1,2,3] Silke Biermann,[2,4] and Philipp Werner[1,5]
[1]*Theoretische Physik, ETH Zurich, 8093 Zürich, Switzerland*
[2]*Centre de Physique Théorique, Ecole Polytechnique, CNRS-UMR7644, 91128 Palaiseau, France*
[3]*Institut de Physique Théorique (IPhT), CEA, CNRS, URA 2306, 91191 Gif-sur-Yvette, France*
[4]*Japan Science and Technology Agency, CREST, Kawaguchi 332-0012, Japan*
[5]*Department of Physics, University of Fribourg, 1700 Fribourg, Switzerland*

We describe a recent implementation of the combined GW and dynamical mean field method ($GW+$DMFT) for the two-dimensional Hubbard model with onsite and nearest-neighbor repulsion. We clarify the relation of the $GW+$DMFT scheme to alternative approaches in the literature, and discuss the corresponding approximations to the free-energy functional of the model. Furthermore, we describe a numerically exact technique for the solution of the $GW+$DMFT equations, namely, the hybridization expansion continuous-time algorithm for impurity models with retarded interactions. We compute the low-temperature phase diagram of the half-filled extended Hubbard model, addressing the metal-insulator transition at small intersite interactions and the transition to a charge-ordered state for stronger intersite repulsions. $GW+$DMFT introduces a nontrivial momentum dependence into the many-body self-energy and polarization. We find that the charge fluctuations included in the present approach have a larger impact on the latter than on the former. Finally, within the $GW+$DMFT framework, as in extended DMFT, the intersite repulsion translates into a frequency dependence of the local effective interaction. We analyze this dependence and show how it affects the local spectral function.

I. INTRODUCTION

Understanding the effects of strong electronic correlations in lattice systems remains a challenge in condensed matter physics. The competition between the tendency of electrons to delocalize due to the resulting gain in kinetic energy and localization by the Coulomb interaction gives rise to a panoply of interesting phenomena, ranging from simple mass enhancements in the sense of Landau theory to charge-, spin-, or orbital-ordering phenomena. To reduce the complexity of the problem, while still keeping the main qualitative effects, e.g., of the delocalization-localization transition, one resorts to low-energy effective models such as the Hubbard or Anderson lattice models. The two-dimensional single-band Hubbard Hamiltonian with a static onsite repulsive interaction U, for example, is believed to describe the physics of the high-temperature superconducting cuprates.[1] Charge-ordering transitions can be captured when an additional intersite interaction term, mimicking the longer-range Coulomb interactions, is retained. This motivates the study of the extended Hubbard model, where charge-ordering effects and screening of the local interactions due to the nonlocal ones are included in addition to the pure Hubbard model physics.

In the paramagnetic phase at half-filling, the Hubbard model exhibits a Mott transition from a metal to a Mott insulator whose spectral function is characterized by a gap at the Fermi energy and Hubbard bands corresponding to atomic-like excitations. This behavior is captured by computational schemes such as the dynamical mean field theory (DMFT) (see Refs. 2 and 3 for reviews) and its extensions [C-DMFT,[4,5] dynamical cluster approximation (DCA),[6] dual fermions,[7] dual bosons,[8] $D\Gamma A$,[9] DMFT$+\Sigma_k$[10]]. A formalism which allows one to treat screening by nonlocal interactions is extended DMFT (EDMFT).[11–15] Its combination with the *ab initio* GW approach[16–18] introduces some momentum dependence into the self-energy, thereby capturing the interplay of screening and nonlocal correlations. This scheme allows for a self-consistent computation of the effective "Hubbard U" in a solid and in principle a fully parameter-free *ab initio* simulation approach for correlated materials. The idea is to take the local part of the self-energy from the EDMFT calculation and supplement it by the nonlocal component of the GW self-energy. A rigorous functional formulation, which is detailed in Sec. II, puts this theory on the same level of mathematical rigor as, e.g., the functional formulation of Hohenberg-Kohn density functional theory.

Despite these promising perspectives, the technical difficulties associated with the numerical treatment of the frequency-dependent effective interaction have for a long time prevented a self-consistent calculation of spectral properties within $GW+$DMFT, even at the model level. Recent progress, both within approximate schemes[19] and numerically exact Monte Carlo techniques,[20,21] is currently giving a new impact to the field.[22–26] In particular, the development of efficient continuous-time Monte Carlo techniques,[27,28] generalized to dynamical interactions in Refs. 20 and 21, now allows for the fully self-consistent solution of the $GW+$DMFT equations, with high enough accuracy to also extract spectral properties.

In this paper, we use these state-of-the-art techniques to study an extended Hubbard model with onsite interaction U and nearest-neighbor repulsive interaction V, and explore the interplay of screening and nonlocal correlations. We show that this model, if solved within the EDMFT framework, captures dynamical screening effects related to the nonlocal interaction V, high-energy satellite features in the one-particle spectra

and, for large V, a transition to a charge-ordered state. We then proceed to study how diagrammatic corrections to EDMFT in the form of momentum-dependent GW contributions to the self-energy modify this picture, and compare the results of self-consistent and non-self-consistent implementations.

The paper is organized as follows: In Sec. II, we discuss the model. In particular, we will show how the Hamiltonian formulation of the problem can be recast into an action or functional formulation. We will explicitly construct two flavors of free-energy functionals whose stationary points would give the exact solution of the model, the first one due to Almbladh *et al.*[29] (see also Ref. 30), the second one constructed by Sun *et al.*[14] In Sec. III, we present different methods of solution: extended DMFT, GW, and combined schemes. We argue that the $GW+\text{DMFT}$ formalism can be derived from the Almbladh free-energy functional, and discuss the differences to the scheme proposed in Ref. 14. The latter stems from another energy functional, which would correspond to a "GD + SOPT + DMFT" method, where D is the boson propagator associated with screening of the nonlocal interaction only, used in a GW-like fashion, supplemented by second-order perturbation theory (SOPT) for the nonlocal effects of the local interaction and dynamical mean field theory for the local ones. Numerical techniques for the solution of the equations are described in Sec. IV and the computational scheme used in this work is summarized in Sec. V. The results of our study are presented in Sec. VI. Section VII contains a summary of our most important findings, and provides perspectives as to how our work inserts itself into the field.

II. MODEL

A. Hamiltonian formulation

We consider the single-band U-V Hubbard model on a two-dimensional square lattice, defined by the grand-canonical Hamiltonian

$$H = -t\sum_{\langle ij\rangle\sigma}(c^\dagger_{i\sigma}c_{j\sigma}+\text{H.c.}) - \mu\sum_i n_i + U\sum_i n_{i\uparrow}n_{i\downarrow} + V\sum_{\langle ij\rangle} n_i n_j, \tag{1}$$

where $c_{i\sigma}$ and $c^\dagger_{i\sigma}$ denote the annihilation and creation operators of a particle of spin $\sigma=\uparrow,\downarrow$ at the lattice site i, $n_{i\sigma}=c^\dagger_{i\sigma}c_{i\sigma}$, and $n_i=n_{i\uparrow}+n_{i\downarrow}$. $\sum_{\langle ij\rangle}$ denotes the sum over nearest-neighbor bonds, $t>0$ is the hopping integral between two neighboring sites, μ is the chemical potential, U the onsite interaction between electrons of opposite spin, and V the interaction between two electrons on neighboring sites, irrespective of their spin. The number of nearest neighbors is $z=2d=4$, where d is the dimension.

With certain approximations, this model can be derived from first principles, as discussed in Appendix A. The limiting case $V=0$ corresponds to the conventional Hubbard model.[31–33] In this study, we will limit ourselves to the paramagnetic phase at half-filling with repulsive interactions $U>0$ and $V>0$.

In the limit of large V, the extended Hubbard model has been shown to display a transition to a charge-ordered state characterized by a freezing of charge carriers and a spatial modulation of the charge density [charge-density wave (CDW)]. This can be explained by a simple energetical argument[34] in the strongly correlated regime ($U\gg t$) at half-filling: while for U much larger than V, electrons will lower their energy by arranging themselves one per site to minimize the onsite repulsion, for V much larger than U, electrons will minimize their off-site repulsion by choosing an arrangement such that one sublattice is occupied by two electrons per site while the other is empty, leading to a commensurate charge order. In the metallic phase ($U\ll t$), the effect of V is more easily understood in terms of screening: the charge fluctuations induced by the V term lead to a reduction of the local effective interaction.

The U-V Hubbard model has been studied in a variety of approximations. An early study in the zero-overlap limit ($U/t\gg 1$) has predicted a phase transition between a Mott insulator and a charge-ordered (CO) insulator at $V_c=U/z$ at zero temperature,[35] while weak-coupling mean field studies have predicted a transition between antiferromagnetic order (AFM, i.e., commensurate SDW) and charge order (i.e., commensurate CDW) at the same boundary.[36,37] This has been confirmed by Monte Carlo calculations in two dimensions.[38] The $V_c=U/z$ boundary has been shown to hold in the $U/V\to 0$ limit as well as in the $U/V\to\infty$ limit by a study at half-filling in the infinite-dimensional limit.[39] Higher-order corrections have been considered in Refs. 40 and 41, leading to a renormalization of the critical temperature and order parameter, as well as the prediction of phase separation in the zero-temperature limit. More recently, variational cluster[42] and two-particle self-consistent approaches[43] have been applied to the U-V Hubbard model.

A first DMFT treatment described the opening of a "pseudogap" and the reentrant behavior of the critical V_c as a function of temperature.[44] In this scheme, the V term only contributed at the Hartree level by shifting the chemical potential since in the limit of infinite dimensions, the contributions beyond Hartree of nonlocal terms vanish, while fluctuations due to local terms such as the onsite Hubbard U do not vanish under rescaling.[45,46] The screening effects contained in the V term are not captured by standard single-site DMFT. Therefore, an extended DMFT (EDMFT) scheme has been proposed to remedy this shortcoming.[11–15] Within this scheme, the nonlocal interactions induce a frequency dependence of the effective local interaction and lead to a sizable *reduction* of the static value of U. In addition, Refs. 14 and 15 showed that one of the consequences of adding a spatially nonlocal contribution to the self-energy is to make the system more insulating.

In this work, we give a precise account of how U and V affect the properties of the local frequency-dependent interactions, and how the latter in turn modify the spectral properties of the system, while systematically investigating the effect of nonlocal GW contributions. We restrict ourselves to the paramagnetic phase at half-filling and will give all energies in units of the half-bandwidth ($4t$). The inverse temperature will be denoted by $\beta=1/T$ ($k_B=1$).

B. Action formulation

The solution of model (1) amounts to computing the Green's functions and other correlation functions. For this

purpose, it is convenient to write the grand-canonical partition function $Z = \mathrm{Tr} e^{-\beta H}$ as a coherent-state path integral[47] $Z = \int \mathcal{D}[c_i^*, c_i] e^{-S}$ where

$$S[c^*,c] = \int_0^\beta d\tau \Big\{ \sum_{ij\sigma} c^*_{i\sigma}(\tau)[(\partial_\tau - \mu)\delta_{ij} + t_{ij}]c_{j\sigma}(\tau) + U \sum_i n_{i\uparrow}(\tau) n_{i\downarrow}(\tau) + \frac{1}{2}\sum_{ij} v^{nl}_{ij} n_i(\tau) n_j(\tau) \Big\}. \tag{2}$$

c_i^* and c_i denote conjugate anticommuting Grassmann fields for site i [$c_i(\tau+\beta) = -c_i(\tau)$], $t_{ij} = -t\delta_{\langle ij\rangle}$, $v^{nl}_{ij} = V\delta_{\langle ij\rangle}$, and $\delta_{\langle ij\rangle} = 1$ if i and j are nearest neighbors and 0 otherwise. τ is the imaginary-time variable. We will denote by $\omega_n = (2n+1)\pi/\beta$ ($\nu_n = 2n\pi/\beta$) the corresponding fermionic (bosonic) Matsubara frequencies. The Fourier transforms of t_{ij} and v^{nl}_{ij} on the lattice are

$$\epsilon_k = -2t[\cos(k_x) + \cos(k_y)], \tag{3}$$

$$v^{nl}_k = 2V[\cos(k_x) + \cos(k_y)]. \tag{4}$$

Using the identity $n_i n_i = 2n_{i\uparrow}n_{i\downarrow} + n_i$, we can rewrite the interaction terms of Eq. (2) as $\frac{1}{2}\sum_{ij} v_{ij} n_i(\tau) n_j(\tau)$ with $v_{ij} = U\delta_{ij} + V\delta_{\langle ij\rangle}$, or

$$v_k = U + v^{nl}_k, \tag{5}$$

provided that we shift the chemical potential $\mu \to \tilde{\mu} = \mu + U/2$. The action hence becomes

$$S[c^*,c] = \int_0^\beta d\tau \Big\{ \sum_{ij\sigma} c^*_{i\sigma}(\tau)\left[(\partial_\tau - \tilde{\mu})\,\delta_{ij} + t_{ij}\right] c_{j\sigma}(\tau) + \frac{1}{2}\sum_{ij} v_{ij} n_i(\tau) n_j(\tau) \Big\}. \tag{6}$$

C. Functional formulation

The problem of finding the solution to the Hamiltonian model (1) or calculating the Green's function corresponding to the action (6) can also be formulated in a functional language. The familiar Luttinger-Ward or Baym-Kadanoff functionals provide examples of such a construction. In the present context, a formulation in terms of the free energy written as a functional of both the Green's function G and the screened Coulomb interaction W is the method of choice since the combined $GW+$DMFT method can naturally be viewed as a specific approximation to such a functional. Indeed, the $GW+$DMFT solution as formulated in Refs. 16 and 17 can be derived as a stationary point (G,W) of the free-energy functional introduced by Almbladh *et al.*,[29] after approximating the correlation part of this functional by a combination of local and nonlocal terms stemming from DMFT and GW, respectively. To draw an illustrative analogy, $GW+$DMFT provides an approximation to the correlation part of the Almbladh free-energy functional, on the same footing as the local density approximation of density functional theory[48] is an approximation to the exchange-correlation part of the Hohenberg-Kohn functional of the energy.

In the literature, several variants of functionals of G and W have been discussed,[14,17,30] and different derivations given. Using a Hubbard-Stratonovich (HS) decoupling as in Ref. 16, we discuss two flavors of free-energy functionals which differ by the choice of the part of the interaction that is decoupled by the HS transformation. The first one reproduces the Ψ functional introduced by Almbladh on which the $GW+$DMFT construction of Ref. 16 is based. The second one is a variant that was used in the study of the extended Hubbard model in Ref. 14.

The Hubbard-Stratonovich transformation[49] relies on the following identity:

$$\exp\left(\frac{1}{2}\int_0^\beta d\tau\, b_i(\tau) A_{ij} b_j(\tau)\right) = \int \frac{\mathcal{D}[x_1(\tau), x_2(\tau), \ldots]}{\sqrt{(2\pi)^N \det A}} \times \exp\left(\int_0^\beta d\tau \left\{ -\frac{1}{2} x_i(\tau)[A^{-1}]_{ij} x_j(\tau) \mp x_i(\tau) b_i(\tau) \right\}\right), \tag{7}$$

where A is a real symmetric positive-definite matrix, $b_i(\tau)$ is a periodic field [$b_i(\tau+\beta) = b_i(\tau)$], $x_i(\tau)$ a real periodic field, and summation over repeated indices is assumed. In the following, we will choose the upper sign for the last term.

Decoupling the whole (local and nonlocal) interaction $\frac{1}{2}\sum_{ij} v_{ij} n_i(\tau) n_j(\tau)$ by the HS transformation corresponds to applying the above formula (7) to the interaction term in Eq. (6), that is, to the choice $b_i \equiv in_i$, $A_{ij} \equiv v_{ij}$, and $x_i \equiv \phi_i$. This choice, denoted as HS-UV in the following, leads to the construction of the Ψ functional as in Almbladh *et al.*[29] and the formalism of Ref. 17. Within the approximation introduced in the next section, this corresponds to the $GW+$DMFT scheme as introduced in Ref. 16. This approach (which was also used in Ref. 15) relies on the argument that the two terms, which represent different matrix elements of the same interaction, should be treated on the same footing.

In Ref. 14, on the other hand, the HS transform has been applied only to the nonlocal interaction term $\frac{1}{2}\sum_{ij} v^{nl}_{ij} n_i(\tau) n_j(\tau)$ in the action (2). This approach, dubbed HS-V in the following, leads to a modified free-energy functional, which we denote by Ψ_V. It was motivated by the aforementioned fact that in the limit of infinite dimensions, with the nonlocal interaction rescaled as $V \to V/z$, the nonlocal term results in a trivial shift of the chemical potential, while the onsite interaction remains nontrivial, justifying a separate treatment for the nonlocal term.

We will first explicitly derive the two functionals Ψ and Ψ_V and, in Sec. VI A, we will compare the results from both decoupling strategies. The results in the reminder of the section, finally, are based on the HS-UV decoupling, that is, on the Ψ functional and the $GW+$DMFT formalism of Ref. 16.

1. "UV decoupling": The Ψ functional

In the HS-UV decoupling scheme, the full interaction term is decoupled via an auxiliary bosonic field ϕ_i. Choosing $b_i \equiv in_i$, $A_{ij} \equiv v_{ij}$, and $x_i \equiv \phi_i$, the transformation (7) applied to

the action (2) leads to

$$S[c^*,c,\phi] = \int_0^\beta d\tau \Big\{ -\sum_{ij\sigma} c^*_{i\sigma}(\tau)\big[\big(G_0^H\big)^{-1}\big]_{ij} c_{j\sigma}(\tau)\Big\} + \int_0^\beta d\tau \times \Big\{\frac{1}{2}\sum_{ij}\phi_i(\tau)[v^{-1}]_{ij}\phi_j(\tau) + i\alpha\sum_i \phi_i(\tau)n_i(\tau)\Big\}, \tag{8}$$

where we introduced the fermionic lattice Hartree Green's function G_0^H defined by $[G_0^{H-1}]_{ij} \equiv [(-\partial_\tau + \mu + \frac{U}{2})\delta_{ij} - t_{ij}]$. For later use, we have moreover inserted a coupling constant α in front of the fermion-boson coupling term. The physically relevant case corresponds to $\alpha = 1$.

The HS transformation replaces an electron-electron interaction by an electron-boson interaction, and introduces a new variable: the auxiliary real boson field ϕ. This has an important consequence: even a first-order diagram in this new interaction contains diagrams of infinite order in the electron-electron interaction. Making even simple approximations on the new action can thus lead to nontrivial diagrams for the original action. Moreover, the electron-boson vertex $i\phi_i n_i$ is *local*. This locality ensures that in the limit of infinite dimensions, the interactions (and in particular V) will contribute beyond the Hartree level.

The generating functional of correlation functions is obtained by introducing the bilinear sources J_f and J_b, coupling to the fermionic and bosonic operators, respectively, so that the action becomes $S[c^*,c,\phi] - S[J_\mathrm{f},J_\mathrm{b}]$, with

$$S[J_\mathrm{f},J_\mathrm{b}] = \int_0^\beta d\tau\, d\tau' \sum_{ij}\Big\{ J_{\mathrm{f},ij}(\tau,\tau')c^*_i(\tau)c_j(\tau') + \frac{1}{2}J_{\mathrm{b},ij}(\tau,\tau')\phi_i(\tau)\phi_j(\tau')\Big\}. \tag{9}$$

The fermionic and bosonic Green's functions for this action are $G_{ij}(\tau-\tau') = -\langle T c_i(\tau)c^*_j(\tau')\rangle = \delta\Omega/\delta J_{\mathrm{f},ij}(\tau,\tau')$ and $W_{ij}(\tau-\tau') = \langle T\phi_i(\tau)\phi_j(\tau')\rangle = -2\delta\Omega/\delta J_{\mathrm{b},ij}(\tau,\tau')$, where we have defined

$$\Omega \equiv -\ln Z[J_\mathrm{f},J_\mathrm{b}] = -\ln \mathrm{Tr} e^{-S[c^*,c,\phi]+S[J_\mathrm{f},J_\mathrm{b}]}. \tag{10}$$

The noninteracting Green's functions (obtained by setting $i\phi_i n_i = 0$) are, respectively, $G|_{\alpha=0}=G_0^H$ and $W(k,i\nu_n)|_{\alpha=0} = [v_k^{-1}]^{-1} = v_k$. This gives a first hint as to the physical meaning of W: without renormalization by the auxiliary bosons, it corresponds to the bare interaction. Coupling to the bosons, which represent density fluctuations of the system, introduces screening into the physical description.

We next perform a Legendre transformation with respect to the sources J_f and J_b,

$$\Gamma[G,W] = \Omega[J_\mathrm{f}[G],J_\mathrm{b}[W]] - \mathrm{Tr}J_\mathrm{f}G + \tfrac{1}{2}\mathrm{Tr}J_\mathrm{b}W, \tag{11}$$

with the reciprocity relations $J_\mathrm{f} = -\frac{\delta\Gamma}{\delta G}$ and $J_\mathrm{b} = 2\frac{\delta\Gamma}{\delta W}$. The physical Green's functions will be obtained by setting $J_\mathrm{f} = 0$ and $J_\mathrm{b} = 0$ or, equivalently, by requiring the stationarity of Γ with respect to G and W.

The free-energy functional Γ can be written as

$$\Gamma_{\alpha=1} = \Gamma_{\alpha=0} + \Psi, \tag{12}$$

where we have defined

$$\Psi \equiv \int_0^1 d\alpha \frac{d\Gamma}{d\alpha}. \tag{13}$$

Γ is the well-known Baym-Kadanoff functional,[50] while Ψ is the extension of the Luttinger-Ward functional $\Phi[G]$ to one- and two-particle propagators.[51]

The noninteracting ($\alpha = 0$) part of the Γ functional is readily evaluated as

$$\Gamma_{\alpha=0} = \mathrm{Tr}\ln(-G) - \mathrm{Tr}\big(G_0^{-1} - G^{-1}\big)G - \tfrac{1}{2}\mathrm{Tr}\ln W + \tfrac{1}{2}\mathrm{Tr}(v^{-1} - W^{-1})W. \tag{14}$$

Indeed, when $\alpha = 0$, the action becomes Gaussian and thus explicitly integrable, namely, $\Omega_{\alpha=0} = -\ln\mathrm{Det}[-G_0^{-1} + J_\mathrm{f}] - \ln(\mathrm{Det}[v^{-1} - J_\mathrm{b}])^{1/2}$. The above definition $G = \delta\Omega/\delta J_\mathrm{f}$ imposes $(G_0^{-1} - J_\mathrm{f})G = 1$ and similarly $(v^{-1} - J_\mathrm{b})W = 1$, yielding Eq. (14). Finally, stationarity of the full Γ implies $\frac{\delta\Gamma}{\delta G} = 0 = \frac{\delta\Gamma_{\alpha=0}}{\delta G} + \frac{\delta\Psi}{\delta G} = G^{-1} - G_0^{-1} + \frac{\delta\Psi}{\delta G}$ for G and $0 = -\frac{1}{2}(W^{-1} - v^{-1}) + \frac{\delta\Psi}{\delta W}$ for W. Defining the self-energies as

$$\Sigma = \frac{\delta\Psi}{\delta G}, \quad \Pi = -2\frac{\delta\Psi}{\delta W} \tag{15}$$

yields Dyson's equations for G and W:

$$G^{-1} = G_0^{-1} - \Sigma, \quad W^{-1} = v^{-1} - \Pi. \tag{16}$$

Being "Ψ derivable," these self-energies will obey global conservation rules.[52]

The above formulation shows that, formally, solving the lattice problem defined by Eq. (2) amounts to evaluating the corresponding Ψ functional, from which G and W can be derived. In Sec. III, we will describe two complementary ways of approximating this functional, EDMFT and GW, before showing how to merge the two approaches, thus arriving at the GW + DMFT free-energy functional.

2. *"V decoupling": The Ψ_V functional*

In the HS-V scheme, proposed in Ref. 14, only the nonlocal interaction term is decoupled via an auxiliary bosonic field ϕ_i. Choosing $b_i \equiv in_i$, $A_{ij} \equiv v^{nl}_{ij}$, and $x_i \equiv \phi_i$, the transformation (7) applied to the action (2) leads to

$$S[c^*,c,\phi] = \int_0^\beta d\tau \Big\{ -\sum_{ij\sigma} c^*_{i\sigma}(\tau)\big[G_0^{-1}\big]_{ij} c_{j\sigma}(\tau) + \alpha U\sum_i n_{i\uparrow}(\tau)n_{i\downarrow}(\tau)\Big\} + \int_0^\beta d\tau \Big\{\frac{1}{2}\sum_{ij}\phi_i(\tau)[(v^{nl})^{-1}]_{ij}\phi_j(\tau) + i\alpha\sum_i\phi_i(\tau)n_i(\tau)\Big\}, \tag{17}$$

where we used the noninteracting fermionic lattice Green's function G_0 defined by $[G_0^{-1}]_{ij} \equiv [(-\partial_\tau + \mu)\delta_{ij} - t_{ij}]$. Again, a coupling constant α was introduced, and the physical case corresponds to $\alpha = 1$. Now, however, the coupling constant is not only a switch for turning on or off the

fermion-boson coupling but at the same time also the local Hubbard interaction.

In principle, the interaction should be a positive-definite matrix in order for the Gaussian integrals invoked in the HS transformation to converge. In contrast to the HS-UV decoupling, where U and V are matrix elements of the screened Coulomb interaction, which is positive definite, this is not the case for the interaction of HS-V, v_{ij}^{nl}. This issue can be dealt with by adding an auxiliary identity matrix multiplied by a large enough constant.[14] In practice, however, the simulation results are not affected by the value of this constant.

As before, the generating functional of correlation functions is obtained by introducing source terms. The fermionic Green's function for this action is unchanged compared to the UV-decoupling case: $G_{ij}(\tau-\tau') = -\langle T c_i(\tau) c_j^*(\tau')\rangle = \delta\Omega/\delta J_{\mathrm{f},ij}(\tau,\tau')$. The bosonic propagator formally still reads $D_{ij}(\tau-\tau') = \langle T\phi_i(\tau)\phi_j(\tau')\rangle = -2\delta\Omega/\delta J_{\mathrm{b},ij}(\tau,\tau')$. It does not, however, correspond to the screened interaction, as in the HS-UV scheme: in the case of vanishing fermion-boson coupling, the bosonic propagator reduces by construction to only the nonlocal part of the bare interaction.

The construction of the free-energy functional Γ proceeds as before by Legendre transformation with respect to the sources J_f and J_b,

$$\Gamma_V[G,D] = \Omega[J_\mathrm{f}[G], J_\mathrm{b}[D]] - \mathrm{Tr} J_\mathrm{f} G + \tfrac{1}{2}\mathrm{Tr} J_\mathrm{b} D, \quad (18)$$

with the reciprocity relations $J_\mathrm{f} = -\frac{\delta\Gamma_V}{\delta G}$ and $J_\mathrm{b} = 2\frac{\delta\Gamma_V}{\delta D}$. The physical Green's functions will be obtained by setting $J_\mathrm{f} = 0$ and $J_\mathrm{b} = 0$ or, equivalently, by requiring the stationarity of Γ_V with respect to G and D. Thanks to the choice of the coupling constant α in front of the interaction and boson-fermion coupling terms $\alpha(U\sum n_{i\uparrow}n_{i\downarrow} + i\sum_i \phi_i n_i)$, Γ_V acquires the same form as before, $\Gamma_{V,\alpha=1} = \Gamma_{V,\alpha=0} + \Psi_V$, with $\Psi_V \equiv \int_0^1 d\alpha \frac{d\Gamma_V}{d\alpha}$, but it is now a functional of G and D.

The noninteracting ($\alpha = 0$) part of the Γ functional reads

$$\Gamma_{V,\alpha=0} = \mathrm{Tr}\ln(-G) - \mathrm{Tr}\big(G_0^{-1} - G^{-1}\big)G - \tfrac{1}{2}\mathrm{Tr}\ln W + \tfrac{1}{2}\mathrm{Tr}[(v^{nl})^{-1} - D^{-1}]D. \quad (19)$$

Finally, stationarity of the full Γ_V reproduces the fermionic Dyson equation for the Green's function and self-energy. For the bosonic part, however, we obtain $0 = -\frac{1}{2}[D^{-1} - (v^{nl})^{-1}] + \frac{\delta\Psi_V}{\delta D}$ for D. The bosonic self-energy

$$\Pi_V = -2\frac{\delta\Psi_V}{\delta D} \quad (20)$$

is thus not equal to the physical polarization of the system.

Again, solving the lattice problem defined by Eq. (2) amounts to evaluating the corresponding Ψ_V functional, from which Σ and Π_V, and in turn G and D, can be derived. Compared to the previous case of the Ψ functional, however, the subtlety of D being the screened nonlocal interaction (not equal to the full W) requires additional care in the construction of a combined DMFT scheme.

III. METHODS OF SOLUTION

A. EDMFT

Ψ is a functional of the fermionic and bosonic Green's functions G_{ij} and W_{ij}. EDMFT replaces this functional by a functional of the local components of the Green's function and screened interaction only. The numerical procedure outlined below thus corresponds to a numerically exact solution of the purely local but otherwise exact $\Phi[G_{ii}, W_{ii}]$. Similarly, the HS-V approach constructs a functional of the local parts of G and D, $\Psi_V[G_{ii}, D_{ii}]$. The local Green's functions can be obtained by solving an auxiliary effective local problem defined by the action

$$S^{\mathrm{EDMFT}}_{\mathrm{eff,HS}\text{-}UV} = -\int_0^\beta d\tau\, d\tau' \sum_\sigma c_\sigma^*(\tau)\mathcal{G}^{-1}(\tau-\tau')c_\sigma(\tau') + \frac{1}{2}\int_0^\beta d\tau\, d\tau' \phi(\tau)\mathcal{U}^{-1}(\tau-\tau')\phi(\tau') + i\int_0^\beta d\tau \phi(\tau) n(\tau), \quad (21)$$

$$S^{\mathrm{EDMFT}}_{\mathrm{eff,HS}\text{-}V} = -\int_0^\beta d\tau\, d\tau' \sum_\sigma c_\sigma^*(\tau)\mathcal{G}^{-1}(\tau-\tau')c_\sigma(\tau') + \int_0^\beta d\tau\, U n_\uparrow(\tau) n_\downarrow(\tau) + \frac{1}{2}\int_0^\beta d\tau\, d\tau' \phi(\tau)\mathcal{D}^{-1}(\tau-\tau')\phi(\tau') + i\int_0^\beta d\tau\, \phi(\tau) n(\tau). \quad (22)$$

These actions are very similar to the lattice actions [Eqs. (8) and (17)], with G_0^H and G_0 replaced by an appropriately defined dynamical $\mathcal{G}$ describing the excursions of an electron in the lattice from a given site (the impurity) and back, and the bare and instantaneous interaction v (or v^{nl} in HS-V) replaced by the retarded interaction $\mathcal{U}$ (or $\mathcal{D}$). The effective actions (21) and (22) are obtained by integrating out all sites but one in the lattice action and taking the infinite-dimensional limit. The derivation of the action for the HS-UV scheme, as well as the EDMFT loop sketched below, are presented in Appendix B.

Integrating out the ϕ field in Eqs. (21) and (22) yields the impurity actions

$$S^{\mathrm{EDMFT}}_{\mathrm{eff,\ HS}\text{-}UV} = -\int_0^\beta d\tau\, d\tau' \sum_\sigma c_\sigma^*(\tau)\mathcal{G}^{-1}(\tau-\tau')c_\sigma(\tau') + \frac{1}{2}\int_0^\beta d\tau\, d\tau' n(\tau)\mathcal{U}(\tau-\tau')n(\tau') - \frac{1}{2}\mathrm{Tr}\ln\mathcal{U}, \quad (23)$$

$$S^{\mathrm{EDMFT}}_{\mathrm{eff,\ HS}\text{-}V} = -\int_0^\beta d\tau\, d\tau' \sum_\sigma c_\sigma^*(\tau)\mathcal{G}^{-1}(\tau-\tau')c_\sigma(\tau') + \int_0^\beta d\tau\, U n_\uparrow(\tau) n_\downarrow(\tau) + \frac{1}{2}\int_0^\beta d\tau\, d\tau' n(\tau)\mathcal{D}(\tau-\tau')n(\tau') - \frac{1}{2}\mathrm{Tr}\ln\mathcal{D}, \quad (24)$$

which feature a retarded interaction $\mathcal{U}(\tau-\tau')$ (for HS-UV) or $\mathcal{D}(\tau-\tau')$ (for HS-V) between charges.

The solution of this impurity problem, described in detail in Sec. IV, requires the calculation of the one-particle Green's

functions $G_{\rm loc} \equiv -\langle T c(\tau) c^*(0)\rangle$ and $W_{\rm loc} \equiv \langle T\phi(\tau)\phi(0)\rangle$ (or $D_{\rm loc}$ for HS-V). From $G_{\rm loc}$ and $W_{\rm loc}$, one computes the corresponding self-energies $\Sigma_{\rm loc} = \mathcal{G}^{-1} - G_{\rm loc}^{-1}$ and $\Pi_{\rm loc} = \mathcal{U}^{-1} - W_{\rm loc}^{-1}$ [or $(\Pi_V)_{\rm loc} = \mathcal{D}^{-1} - D_{\rm loc}^{-1}$]. The EDMFT approximation identifies the impurity self-energies with the lattice self-energies: $\Sigma(k,i\omega_n) \approx \Sigma_{\rm loc}(i\omega_n)$, $\Pi(k,i\nu_n) \approx \Pi_{\rm loc}(i\nu_n)$ [or $(\Pi_V)_{\rm loc}(i\nu_n)$]. This allows one to evaluate (approximate) lattice Green's functions $G(k,i\omega_n)$ and $W(k,i\nu_n)$ [or $D(k,i\nu_n)$] through Dyson's equation and estimates of the local lattice Green's functions by summation over k. Eventually, one obtains updated $\mathcal{G}$ and $\mathcal{U}$ (or $\mathcal{D}$) via

$$\mathcal{G}^{-1} = G_{\rm loc}^{-1}[\Sigma_{\rm loc}] + \Sigma_{\rm loc}, \tag{25}$$

$$\mathcal{U}^{-1} = W_{\rm loc}^{-1}[\Pi_{\rm loc}] + \Pi_{\rm loc}, \tag{26}$$

$$\mathcal{D}^{-1} = D_{\rm loc}^{-1}[(\Pi_V)_{\rm loc}] + (\Pi_V)_{\rm loc}. \tag{27}$$

B. *GW* approximation

While EDMFT can treat strong local correlations, it completely neglects the nonlocal contributions to the self-energy. A complementary approach, which treats spatial fluctuations, but works reliably only in the weakly correlated regime, is the GW method.[53–55] The GW approximation has been used extensively to investigate the properties of weakly correlated materials, such as the band gaps of semiconductors and is nowadays implemented in several different electronic structure codes (see, e.g., Refs. 56 and 57). In these materials, GW correctly accounts for the screening effects of the electrons at the random-phase approximation (RPA) level. Schematically, for a general Coulomb interaction $v(r) \sim 1/r$, one-shot GW replaces the bare interaction v of the Fock self-energy $\Sigma_F \sim G_0 v$ by the screened interaction $W = v/\epsilon_{\rm RPA}$, where $\epsilon_{\rm RPA} = 1 - vP_0$ and $P_0 \sim G_0 G_0$ is the dynamical Lindhard function. In a self-consistent scheme, G_0 is replaced by the interacting Green's function G.[58] The Fock self-energy thus becomes $\Sigma_{GW} \sim GW$, hence the name of the approximation. Formally, the GW approximation can be obtained by Hubbard-Stratonovich decoupling the Coulomb interaction v *via* an auxiliary bosonic field ϕ characterized by the propagator $W \sim \langle\phi\phi\rangle$. This amounts to replacing the electron-electron interaction by the indirect interaction of two electrons mediated by a boson described by ϕ. The first-order self-energy diagram in the expansion of this electron-boson interaction is $\Sigma \sim GW$.

The standard derivation of the GW approximation relies on a truncation of Hedin's equations,[53] where the three-legged vertex $\Lambda = 1 + \frac{\delta\Sigma}{\delta G} GG\Lambda$ is set to unity. In the following, we will derive the GW approximation for our lattice model in a diagrammatic way based on the four-legged vertices of standard perturbation theory for both free-energy functionals, that is, both choices of the HS decoupling. In the HS-V approach, the lattice action of Eq. (8) contains two interaction vertices: a local electron-electron interaction $U n_{i\uparrow} n_{i\downarrow}$ and a local electron-boson interaction $i\phi_i n_i$. Consequently, the perturbation expansion of the Green's function will contain two types of bare interaction vertices, namely, $\Gamma^{(0)}_{\rm ee}(\tau_1,\tau_2,\tau_3,\tau_4)_{ijkl} = U\delta_{ijkl}\delta_{i\uparrow}\delta_{j\downarrow}\delta_{k\uparrow}\delta_{l\downarrow}\delta(\tau_1 - \tau_2)\delta(\tau_3 - \tau_4)\delta(\tau_2 - \tau_3)$ and $\Gamma^{(0)}_{\rm eb}(\tau_1,\tau_2,\tau_3)_{ijk} = i\delta_{ijk}\delta(\tau_1 - \tau_2)\delta(\tau_3 - \tau_2)$, which we will represent as shown in Figs. 1 and 2. We will suppose that we can perform the expansions separately and then sum the two results (which is an approximation since there could well be sequences of interactions with alternating $\Gamma^{(0)}_{\rm ee}$ and $\Gamma^{(0)}_{\rm eb}$). In the HS-UV approach, there is only the electron-boson vertex $\Gamma^{(0)}_{\rm eb}$.

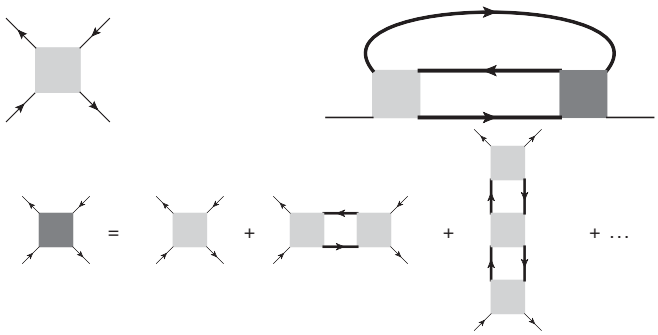

FIG. 1. Diagrammatic expansion of the electron-electron vertex. From left to right, top to bottom: Bare electron-electron interaction vertex $\Gamma^{(0)}_{\rm ee}$. Fully boldified $\Sigma_{\rm ee}$. Expansion of the full electron-electron vertex $\Gamma_{\rm ee}$.

The vertex $\Gamma^{(0)}_{\rm ee}$ will lead to contributions that are not present in the HS-UV decoupling scheme. The perturbation expansion in powers of $\Gamma^{(0)}_{\rm ee}$ yields a series of self-energy diagrams, the lines of which are noninteracting Green's functions G_0. Since some higher-order diagrams contain "self-energy insertions," the number of diagrams can be reduced by "boldifying" the lines, namely, by replacing G_0 by the interacting Green's function G. Subsequently, the number of diagrams can be further reduced by regrouping the interaction vertices into a "boldified" vertex $\Gamma_{\rm ee}$ pictured in Fig. 1. Thus, the electron-electron part of the self-energy (beyond the Hartree self-energy) can be described (Fig. 1) by the exact expression[60]

$$\Sigma_{\rm ee} = -\Gamma^{(0)}_{\rm ee} GGG\Gamma_{\rm ee}, \tag{28}$$

with bold propagators G *and* bold vertices $\Gamma_{\rm ee}$. Note that only the right vertex is boldified to avoid double counting. This

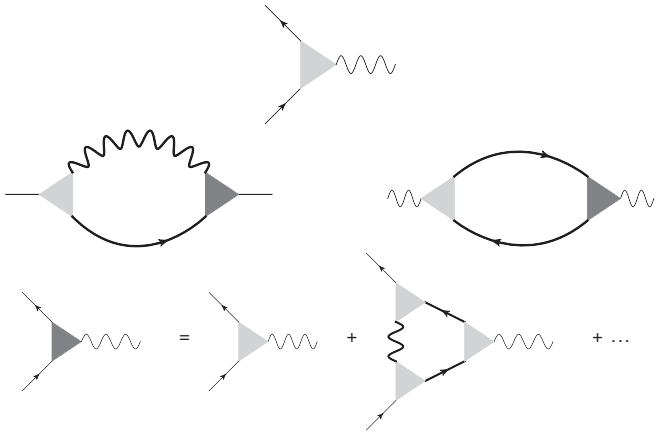

FIG. 2. Diagrammatic expansion of the electron-boson vertex. From left to right, top to bottom: Bare electron-boson interaction vertex $\Gamma^{(0)}_{\rm eb}$. Fully boldified $\Sigma_{\rm eb}$. Fully boldified Π. Expansion of the full electron-boson vertex $\Gamma_{\rm eb}$.

vertex is also called the fully reducible vertex. We stress that this electron-electron contribution to the electronic self-energy is absent in the HS-UV approach since in this scheme there is no longer any electron-electron interaction vertex after the HS decoupling.

Similarly, the expansion of the partition function in powers of $\Gamma_{\rm eb}^{(0)}$ can be simplified by boldifying the G_0 and W_0 ($=v$ or v^{nl}) lines and the vertices, leading to graphs of the form displayed in Fig. 2, corresponding to the expressions

$$\Sigma_{\rm eb} = \Gamma_{\rm eb}^{(0)} G W \Gamma_{\rm eb}, \tag{29}$$

$$\Pi_{\rm eb} = -2\Gamma_{\rm eb}^{(0)} G G \Gamma_{\rm eb}. \tag{30}$$

The expansion for the bold electron-boson vertex $\Gamma_{\rm eb}$ is also pictured in Fig. 2.

The usual GW approximation truncates the expansion of the electron-boson vertex function $\Gamma_{\rm eb}$ after its first term, namely, by taking $\Gamma_{\rm eb} \approx \Gamma_{\rm eb}^{(0)} = i\delta$. This simplification, which amounts to neglecting the so-called vertex corrections, yields the familiar expressions $\Sigma_{\rm eb}^{GW} = -GW$ and $\Pi^{GW} = 2GG$.[61] For the HS-UV decoupling, $\Sigma = \Sigma_{\rm eb}$ and thus

$$\Sigma_{\text{HS-}UV}^{GW} = -GW. \tag{31}$$

For the HS-V decoupling, there is a second contribution coming from the electron-electron vertex. If one approximates $\Gamma_{\rm ee} \approx \Gamma_{\rm ee}^{(0)}$ (as in Ref. 14), one gets $\Sigma_{\rm ee}^{GW} = -U^2 GGG$, and hence

$$\Sigma_{\text{HS-}V}^{GW} = -GD - U^2 GGG. \tag{32}$$

At this point, a few remarks are in order: the two approximations (31) and (32) are not equivalent. Making the lowest-order approximation on the electron-electron vertex is a stronger assumption than truncating the electron-boson vertex. In the HS-V approach, the series of diagrams corresponding to Eq. (32) contains the ring of "bubbles" made up of G and v_{ij}^{nl} (which contains only the off-site repulsion V), plus a second-order diagram in U. In contrast, the diagrams in $\Sigma_{\text{HS-}UV}^{GW}$ contain the ring of bubbles made up of G and v_{ij} (which contains U and V). Put differently, it not only comprises the off-site interaction V to all orders (at the RPA level), but also the onsite interaction U to all orders (at the RPA level). We thus expect the HS-UV scheme to be better poised to capture nonlocal effects arising from V *and* U, while the HS-V scheme will probably give nontrivial contributions only in parameter regimes where V plays the dominant role. Therefore, while benchmarking both approaches in the results section, we will focus on the formulation in terms of the Almbladh functional in the following discussion of the combined GW + DMFT scheme. A similar combination based on the Ψ_V functional is possible, leading to a combination of the GD plus self-consistent second-order perturbation theory expression of Eq. (32) with dynamical mean field theory, as described in Ref. 14. We refer to this combination in the following as "GD + SOPT + DMFT".

C. GW + DMFT approach

As already hinted at before, EDMFT and GW are complementary approximate schemes: EDMFT provides a good description of local correlations, while GW captures longer-range correlations and in particular long-range screening. Therefore, combining both approximations appears promising. The GW + DMFT approach[16,17] makes an approximation on $\Psi[G_{ij}, W_{ij}]$ by decomposing it in the following way:

$$\Psi \approx \Psi^{\rm EDMFT}[G_{ii}, W_{ii}] + \Psi_{\rm nonloc}^{GW}[G_{ij}, W_{ij}], \tag{33}$$

where $\Psi_{\rm nonloc}^{GW} = \Psi^{GW} - \Psi_{\rm loc}^{GW}$.

While EDMFT will generate the series of local self-energy diagrams up to infinite order, the nonlocal contributions to Ψ will be generated in a perturbative way by the nonlocal part of the GW diagrams, thus avoiding double counting.

In the limit of infinite dimensions, nonlocal diagrams vanish. Thus, the effect (if any) of the nonlocal contributions is expected to manifest itself only as the dimension is lowered. The proximity to a phase transition should also enhance spatial fluctuations. In principle, the GW contribution should nonetheless remain a correction to the DMFT part, which justifies why $\Psi_{\rm nonloc}[G_{ij}, W_{ij}]$ can be treated on a perturbative level, while $\Psi[G_{ii}, W_{ii}]$ is evaluated to all orders.

The approximate electronic self-energy will be given by $\Sigma_{ij} = \Sigma_i^{\rm loc}\delta_{ij} + (1-\delta_{ij})\Sigma_{ij}^{GW}$. The $1-\delta_{ij}$ factor ensures that only the nonlocal part of the GW self-energy is added. Analogous expressions hold for Π_{ij}. This approach is very general. In the specific case of the extended Hubbard model, one can expect the GW contribution to become significant as one approaches an instability in the charge sector, namely, close to the charge-ordering transition. The GW diagrams can in principle be replaced by other perturbative diagrammatic corrections, corresponding to a decoupling of the interaction in other channels.

IV. NUMERICAL IMPLEMENTATION

A. Solution of the EDMFT impurity problem

The impurity models (23) and (24) can be solved efficiently using the hybridization-expansion continuous-time quantum Monte Carlo solver (CTQMC-hyb).[27] The formalism has been previously derived using a Hamiltonian representation of the impurity model.[20,21] Here, we discuss an alternative derivation based on the effective action, focusing on the case of action (23). A CTQMC-hyb simulation samples configurations representing specific time sequences of "hybridization events," with weight proportional to the determinant of a matrix of hybridization functions. The perturbation expansion of the partition function Z and the summation of diagrams with identical operator sequences leads to

$$\begin{aligned} Z = \sum_{\{n_\sigma\}=0}^{\infty} \prod_\sigma \Bigg[\frac{1}{(n_\sigma!)^2} \int_0^\beta d\tau_1^\sigma \int_0^\beta d\tau_1'^\sigma \dots \\ \times \int_0^\beta d\tau_{n_\sigma}^\sigma \int_0^\beta d\tau_{n_\sigma}'^\sigma \mathrm{Det}\Delta_\sigma \Bigg] \int D[c^*,c] e^{-S_{at}} T \\ \times \prod_\sigma c_\sigma^*(\tau_1'^\sigma) c_\sigma(\tau_1^\sigma) \dots c_\sigma^*(\tau_{n_\sigma}'^\sigma) c_\sigma(\tau_{n_\sigma}^\sigma), \end{aligned} \tag{34}$$

where $(\Delta_\sigma)_{ij} = \Delta_\sigma(\tau_i - \tau_j')$ is the hybridization function evaluated for the time difference between annihilation operator

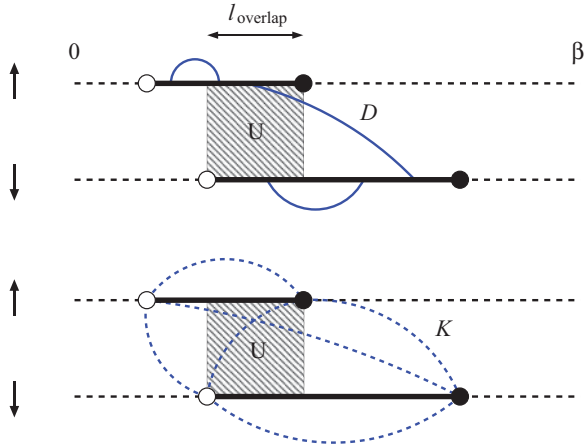

FIG. 3. (Color online) Illustration of a Monte Carlo configuration in the segment representation. The top figure corresponds to a configuration with one spin-up and one spin-down segment, each representing a time interval marked by a creation operator (empty circle) and an annihilation operator (full circle). The overlap of the segments, corresponding to the width of the hashed region, yields the weight due to the instantaneous interaction U. The retarded interaction $\mathcal{D}(\tau-\tau')$ is represented by the blue curved lines. The bottom panel represents the weight of this configuration after integration of the retarded interaction over the segments. The dashed blue lines correspond to the interaction $K(\tilde{\tau}_i-\tilde{\tau}_j)$ between creation and annihilation operators.

i and creation operator j and

$$S_{at} = \frac{1}{2}\sum_{\sigma\sigma'}\int\int d\tau\, d\tau' n_\sigma(\tau)\mathcal{U}_{\sigma\sigma'}(\tau-\tau')n_{\sigma'}(\tau') + \int d\tau \sum_\sigma c_\sigma(\tau)^*\left(\partial_\tau-\mu\right)c_\sigma(\tau) \tag{35}$$

represents the interaction and chemical potential contributions of action (23). The interaction $\mathcal{U}$ can always be split into a delta-function contribution and a nonsingular contribution $\mathcal{U}(\tau)_{\sigma\sigma'} = U\delta(\tau)(1-\delta_{\sigma\sigma'}) + \mathcal{D}(\tau)_{\sigma\sigma'}$. (In the HS-$V$ scheme, this separation is already explicit.) The last factor of Eq. (34) can be easily evaluated since the time-evolution operators are diagonal in the occupation-number basis. In the segment representation,[27] each imaginary-time interval with occupation $n_\sigma = 1$ is marked by a segment, and the last factor can (up to a permutation sign) be written as $w_\mu w_U w_\mathcal{D}$ with $w_\mu = e^{\mu(l_\uparrow+l_\downarrow)}$ and $w_U = e^{-Ul_{\text{overlap}}}$. Here, l_σ stands for the total length of segments of spin σ, while l_{overlap} is the total overlap between segments of opposite spin (see illustration of a segment configuration in Fig. 3). The retarded interaction contributes a factor

$$w_\mathcal{D} = e^{-\frac{1}{2}\sum_{\sigma_1\sigma_2}\int_0^\beta d\tau_1\int_0^\beta d\tau_2\mathcal{D}(\tau_1-\tau_2)_{\sigma_1\sigma_2}n_{\sigma_1}(\tau_1)n_{\sigma_2}(\tau_2)} = \exp\left(-\frac{1}{2}\sum_{\substack{\sigma_1\sigma_2\\ k_{\sigma_1}k_{\sigma_2}}}\int_{\tau'_{k_{\sigma_1}}}^{\tau_{k_{\sigma_1}}} d\tau_1\int_{\tau'_{k_{\sigma_2}}}^{\tau_{k_{\sigma_2}}} d\tau_2\mathcal{D}(\tau_1-\tau_2)_{\sigma_1\sigma_2}\right), \tag{36}$$

where $\{k_\sigma\}$ represents the collection of segments of spin σ.

Let us now define a function $K(\tau)$ such that $K''(\tau) = \mathcal{D}(\tau)$ for $0<\tau<\beta$ and $K(0^+) = K(\beta^-) = 0$. K is β periodic and symmetric around $\tau=\beta/2$. It has a slope discontinuity at zero, so that the second derivative also gives a delta-function contribution. In the interval $[0,\beta]$,

$$K(\tau) = \frac{1}{\beta}\sum_{n\neq 0}\frac{\mathcal{D}(i\nu_n)-\mathcal{D}(0)}{(i\nu_n)^2}(e^{i\tau\nu_n}-1). \tag{37}$$

Carrying out the integral in Eq. (36) thus yields

$$\ln w_\mathcal{D} = -\frac{1}{2}\sum_{\substack{\sigma_1\sigma_2\\ k_{\sigma_1}k_{\sigma_2}}}\left[-K\left(\tau'_{k_{\sigma_1}}-\tau'_{k_{\sigma_2}}\right)+K\left(\tau_{k_{\sigma_1}}-\tau'_{k_{\sigma_2}}\right) + K\left(\tau'_{k_{\sigma_1}}-\tau_{k_{\sigma_2}}\right)-K\left(\tau_{k_{\sigma_1}}-\tau_{k_{\sigma_2}}\right)\right] + K'(0)(l_\uparrow+l_\downarrow)+2K'(0)l_{\text{overlap}}. \tag{38}$$

Using the fact that $K(\tau)$ is an even function, we can write $\ln w_\mathcal{D} = \sum_{i>j}s_i s_j[K(\tilde{\tau}_i-\tilde{\tau}_j)-K(0)] + K'(0)(l_\uparrow+l_\downarrow)+2K'(0)l_{\text{overlap}}$ where the time arguments of the hybridization events (creation and annihilation operators) are now ordered as $0<\tilde{\tau}_1<\tilde{\tau}_2<\ldots<\beta$ and s is $+1$ for a creation operator and -1 for an annihilation operator.

We conclude that the retarded part of the interaction, $\mathcal{D}(\tau-\tau')$, results in a retarded "interaction" between all pairs of impurity creation and annihilation operators, as well as a shift of the instantaneous interaction $U\to\tilde{U}=U-2K'(0)$ and a shift of the chemical potential $\mu\to\tilde{\mu}=\mu+K'(0)$. If one writes the interaction term in terms of density fluctuations, $\frac{1}{2}\iint\bar{n}(\tau)\mathcal{D}(\tau-\tau')\bar{n}(\tau')$ with $\bar{n}=n-\langle n\rangle$, the only change induced in the weight is yet another shift of the chemical potential $\tilde{\mu}=\mu+K'(0)-2\langle n\rangle K'(0)$. The retarded interactions can be evaluated at negligible computational cost since the calculation of this contribution for a local update is $O(n)$ (where n is the number of operators), while the evaluation of a determinant ratio is $O(n^2)$.

In practice, the local bosonic propagator $W_{\text{loc}} = \langle T\phi(\tau)\phi(0)\rangle$ needed in Eq. (26) is deduced from the connected charge-charge correlation function $\chi_{\text{loc}} = \langle T\bar{n}(\tau)\bar{n}(0)\rangle$ via the relation

$$W_{\text{loc}}(i\nu_n) = \mathcal{U}(i\nu_n) - \mathcal{U}(i\nu_n)\chi_{\text{loc}}(i\nu_n)\mathcal{U}(i\nu_n). \tag{39}$$

Indeed, using Eq. (21), W_{loc} can be reexpressed as $W_{\text{loc}} = -2\frac{\delta\ln Z}{\delta\mathcal{U}^{-1}}$. The chain rule $\frac{\delta\ln Z}{\delta\mathcal{U}^{-1}} = -\mathcal{U}\frac{\delta\ln Z}{\delta\mathcal{U}}\mathcal{U}$ and Eq. (23) give $\frac{\delta\ln Z}{\delta\mathcal{U}} = -\frac{1}{2}\chi_{\text{loc}}+\frac{1}{2}\mathcal{U}^{-1}$, and hence one arrives at Eq. (39). An analogous expression holds for D_{loc}.

B. Self-consistency

The GW + EDMFT scheme is generally expected to work well if the nonlocal GW contribution to the self-energy is a relatively small correction to the local self-energy computed by EDMFT. It thus makes sense to first obtain a reasonable guess of the final solution by applying EDMFT only, and then compute the nonlocal correction and study its effect on the properties of the system. Following this observation, we implemented the GW + EDMFT scheme as follows: for a given U and V, we (i) obtain a converged EDMFT solution, (ii) take the EDMFT solution as the starting point for a

self-consistent GW + EDMFT calculation, and (iii) stop when local and nonlocal observables have converged.

This is not the only possible combination of EDMFT with GW, although the final result of the self-consistent scheme should not depend on the starting point, provided the scheme converges. For instance, one can choose to initialize the scheme by computing Σ^{GW} and Π^{GW} from the noninteracting propagators $G_0(k,i\omega_n) = [i\omega_n + \mu - \epsilon(k)]^{-1}$ and $W_0(k,i\nu_n) = v_k$. Yet, these propagators yield a very large GW polarization owing to their metallic character (they correspond to the $U = 0$, $V = 0$ case). Especially for the regions of interest here (V close to V_c and finite U), this large polarization is far from the expected solution. Indeed, one can observe that when taking an insulating G and, e.g., $W = v$ as inputs for GW, the resulting polarization is small compared to the local polarization Π_{loc}.

C. Analytical continuation

The nontrivial structures of the frequency-dependent interaction result in additional features in the local spectral function $A(\omega) = -\frac{1}{\pi}\text{Im}G(\omega + i\eta)$. For example, the case $\text{Im}\mathcal{D}(\omega) = -\lambda^2[\delta(\omega - \omega_0) - \delta(\omega + \omega_0)]$, studied in Ref. 21, corresponds to the Holstein-Hubbard model, for which the local spectral function is expected to display plasmonic peaks at multiples of the "plasmon" frequency ω_0.[19] However, the commonly used maximum entropy (MaxEnt) analytical continuation[62] tends to smooth out high-energy features and therefore a dedicated scheme must be implemented to recover the sought-after features. A solution to this problem has been proposed in Ref. 19, inspired from the exact expression of the Green's function in the atomic limit.[63] We thus proceed as follows: (a) From $\mathcal{U}(i\nu_n)$ (or, equivalently, $\mathcal{D}$), we compute the bosonic function $B(\tau) = \exp[-K(\tau)]$, its Fourier transform $B(i\nu_n)$ and, using a Padé procedure,[64] its spectral function $B(\omega)$. (b) From $G(\tau)$, we compute an auxiliary function $G_{\text{aux}}(\tau) = G(\tau)/B(\tau)$ and use MaxEnt to obtain $A_{\text{aux}}(\omega)$. (c) Finally, we compute the spectral function as the convolution

$$A(\omega) = \int_{-\infty}^{\infty} d\epsilon\, B(\epsilon)\frac{1 + e^{-\beta\omega}}{(1 + e^{\beta(\epsilon-\omega)})(1 - e^{-\beta\epsilon})}A_{\text{aux}}(\omega - \epsilon). \tag{40}$$

V. SUMMARY OF THE COMPUTATIONAL SCHEME

The computational scheme can be summarized as follows for the HS-UV [resp. HS-V] decoupling:

(1) Start with an initial guess for $\Sigma(k,i\omega)$ and $\Pi(k,i\nu)$: for instance, $\Sigma = 0$ and $\Pi = 0$ (noninteracting limit).

(2) *Lattice Green's functions*. Compute $G(k,i\omega)$ and $W(k,i\nu)$ [resp. $D(k,i\nu)$] *via* Dyson's equation with v_k [resp. v_k^{nl}] as the bare interaction.

(3) *EDMFT self-consistency*. Extract $G_{\text{loc}}(i\omega) = \sum_k G(k,i\omega)$ and $W_{\text{loc}}(i\nu) = \sum_k W(k,i\nu)$ [resp. D_{loc}] and use Eqs. (25) and (26) to find $\mathcal{G}(i\omega)$ and $\mathcal{U}(i\nu)$ [resp. $\mathcal{D}(i\nu)$].

(4) *Impurity solver*. Compute $G_{\text{loc}}(\tau)$ and $\chi_{\text{loc}}(\tau)$ [resp. $\chi^V_{\text{loc}}(\tau)$], as well as $W_{\text{loc}} = \mathcal{U} - \mathcal{U}\chi_{\text{loc}}\mathcal{U}$ [resp. $D_{\text{loc}} = \mathcal{D} - \mathcal{D}\chi^V_{\text{loc}}\mathcal{D}$]. From these, extract the self-energies $\Sigma_{\text{loc}} = \mathcal{G}^{-1} - G^{-1}_{\text{loc}}$ and $\Pi_{\text{loc}} = \mathcal{U}^{-1} - W^{-1}_{\text{loc}}$ [resp. $(\Pi_V)_{\text{loc}} = \mathcal{D}^{-1} - D^{-1}_{\text{loc}}$].

(5) *GW + DMFT step (optional)*.

(a) Compute

$$\Pi^{GW}(k,\tau) = 2\sum_q G(q,\tau)G(q-k,-\tau),$$

$$\Sigma^{GW}(k,\tau) = -\sum_q G(q,\tau)W^c(k-q,\tau) + \sum_q G(q,0)v(k-q),$$

where $W^c = W - v$ is the regular part of W. Respectively, for HS-V,

$$\Sigma^{GW}(k,\tau) = -\sum_q G(q,\tau)D(k-q,\tau), - U^2\sum_q G(q,\tau)\Pi^{GW}(q-k,\tau).$$

(b) Extract nonlocal parts from GW:

$$\Sigma^{GW}_{\text{nonloc}}(k,i\omega) = \Sigma^{GW}(k,i\omega) - \sum_k \Sigma(k,i\omega),$$

$$\Pi^{GW}_{\text{nonloc}}(k,i\nu) = \Pi^{GW}(k,i\nu) - \sum_k \Pi(k,i\nu).$$

(c) Combine $\Sigma_{\text{loc}}(i\omega)$ and $\Sigma^{GW}_{\text{nonloc}}(k,i\omega)$ into $\Sigma(k,i\omega)$, as well as $\Pi_{\text{loc}}(i\nu)$ and $\Pi^{GW}_{\text{nonloc}}(k,i\nu)$ into $\Pi(k,i\nu)$.

(6) Go back to step 2 until convergence.

In a pure EDMFT scheme, steps 5(a)–(c) are skipped. Note that the decomposition of W into W^c and v in 5(a) is aimed at suppressing the singular part of W, namely, in the limit of infinite frequency, W goes to a finite value v, whereas W^c vanishes, making the Fourier transform of the latter well defined. Figure 4 gives an overview of the implementation of the GW + DMFT scheme.

VI. RESULTS

In this section, we present numerical results for the half-filled U-V Hubbard model on a two-dimensional square lattice using the different approximate formalisms discussed in the previous sections. We solve the impurity problems using the CTQMC-hyb method. Unless otherwise stated, the computations are performed at inverse temperature $\beta = 100$ (we use the half-bandwidth $4t$ as the unit of energy). The k sums are discretized in the irreducible Brillouin zone on a 80×80 grid, while the imaginary-time correlation functions are measured on a grid of $N = 1000$ equally spaced points. Up to 40 EDMFT steps are required to reach convergence close to the Mott transition.

A. Phase diagram

Figure 5 shows the phase diagram in the space of the parameters U and V for the two decoupling schemes HS-UV and HS-V. The top panel shows the EDMFT result, the bottom panel corresponds to GW + DMFT. There are three phases: (i) a Fermi liquid (FL) metal at small U and small V, (ii) a charge-ordered (CO) insulator at small U and large V, and (iii) a Mott insulating (MI) phase at large U and small V.

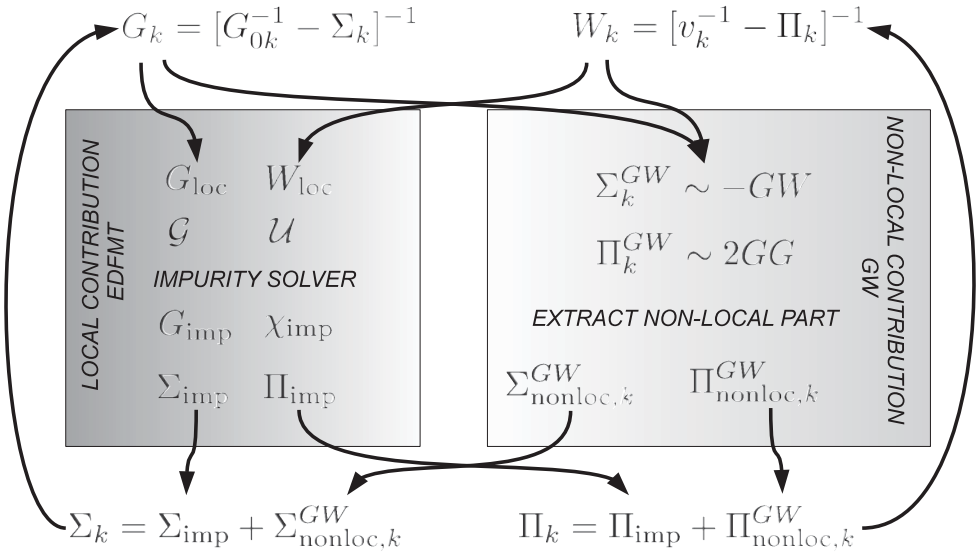

FIG. 4. Computational scheme (HS-UV decoupling).

The phase boundary to the charge-ordered phase has been located by approaching the phase transition from below V_c.

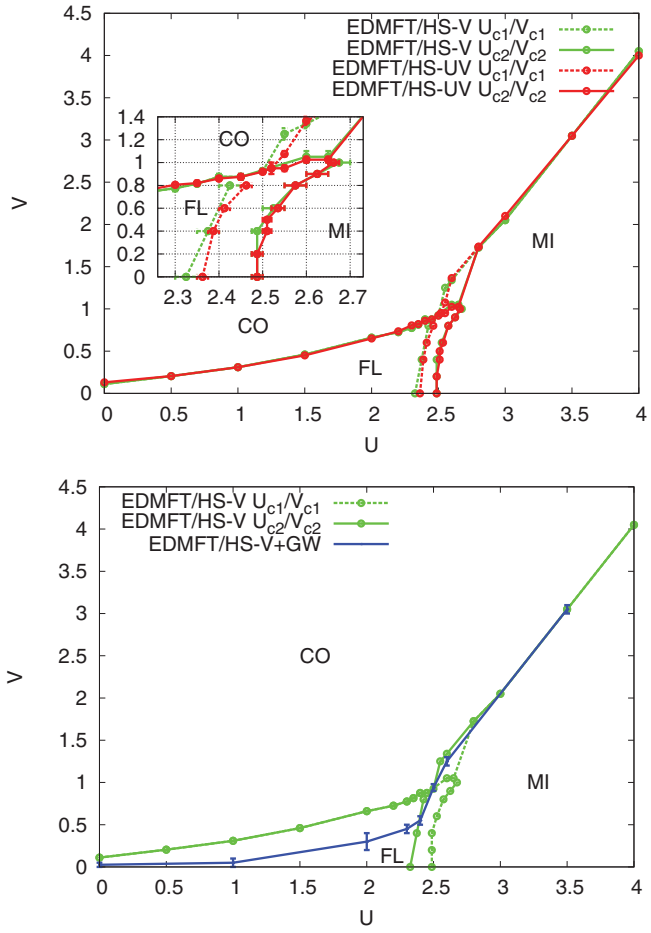

FIG. 5. (Color online) Phase diagram of the U-V Hubbard model for HS-UV (red), and HS-V (green) decoupling at $\beta = 100$. The top panel shows the EDMFT result, and the bottom panel compares the GW + EDMFT result for the HS-V scheme to EDMFT.

The phase transition corresponds to a diverging charge susceptibility, namely, to the formation of a pole in the Fourier transform $\chi(k,\omega)$ of $\chi_{ij}(t-t') \equiv \partial\langle n_i(t)\rangle/\partial h_j(t')$, where $h_j(t)$ is a probe field. Specifically, the charge-ordering transition will be signaled by a divergence at $Q = (\pi,\pi)$ and $\omega = 0$ since the probe field for this phase is $h_i(t) = he^{iQR_i}$. Using the action (2), one can easily show that $\chi_{ij}(t-t') = \langle \bar{n}_i(t)\bar{n}_j(t')\rangle$. Recalling that $W = v - v\chi v$, we find the exact relation

$$\chi(k,\omega) = -\frac{\Pi(k,\omega)}{1 - v_k\Pi(k,\omega)} \tag{41}$$

for the HS-UV scheme. Similarly, for the HS-V scheme, χ_V can be computed from $D = v^{nl} - v^{nl}\chi_V v^{nl}$ or $\chi_V = -\Pi_V/(1 - v^{nl}\Pi_V)$. This shows that the transition also corresponds to the appearance of a pole in the fully screened interaction $W(k,i\nu_n)$, and provides a rigorous definition of V_c for HS-UV and HS-V, respectively:

$$1 - (U - 4V_c)\Pi\,[k = (\pi,\pi), \omega = 0] = 0, \tag{42}$$

$$1 + 4V_c\Pi_V\,[k = (\pi,\pi), \omega = 0] = 0. \tag{43}$$

On the other hand, the phase boundary between the metal and the Mott insulator is signaled by a vanishing spectral weight at the Fermi level, which is related to the imaginary-time Green's function by $A_{T\to 0}(\omega = 0) = \lim_{\beta\to\infty} \frac{\beta}{2} G(\frac{\beta}{2})$. The curvature of the FL-MI phase boundary shows that increasing the nearest-neighbor repulsion V makes the system more metallic.

Within EDMFT, both decoupling schemes yield very similar phase diagrams. In the temperature range $\beta \in [25,100]$, the phase diagram also does not depend much on temperature. The boundary of the charge-ordered phase is characterized by two main regimes: for $U < U_c \approx 2.5$, $dV_c/dU \approx \frac{1}{4}$, which is the prediction of mean-field studies. For $U > U_c$, $dV_c/dU \approx 2$. The transition between the two regimes is marked by a kink. This kink also coincides with the point where the charge-ordered critical line meets the Mott critical line $U_c(V)$. The latter is only weakly dependent on V. The sudden change of

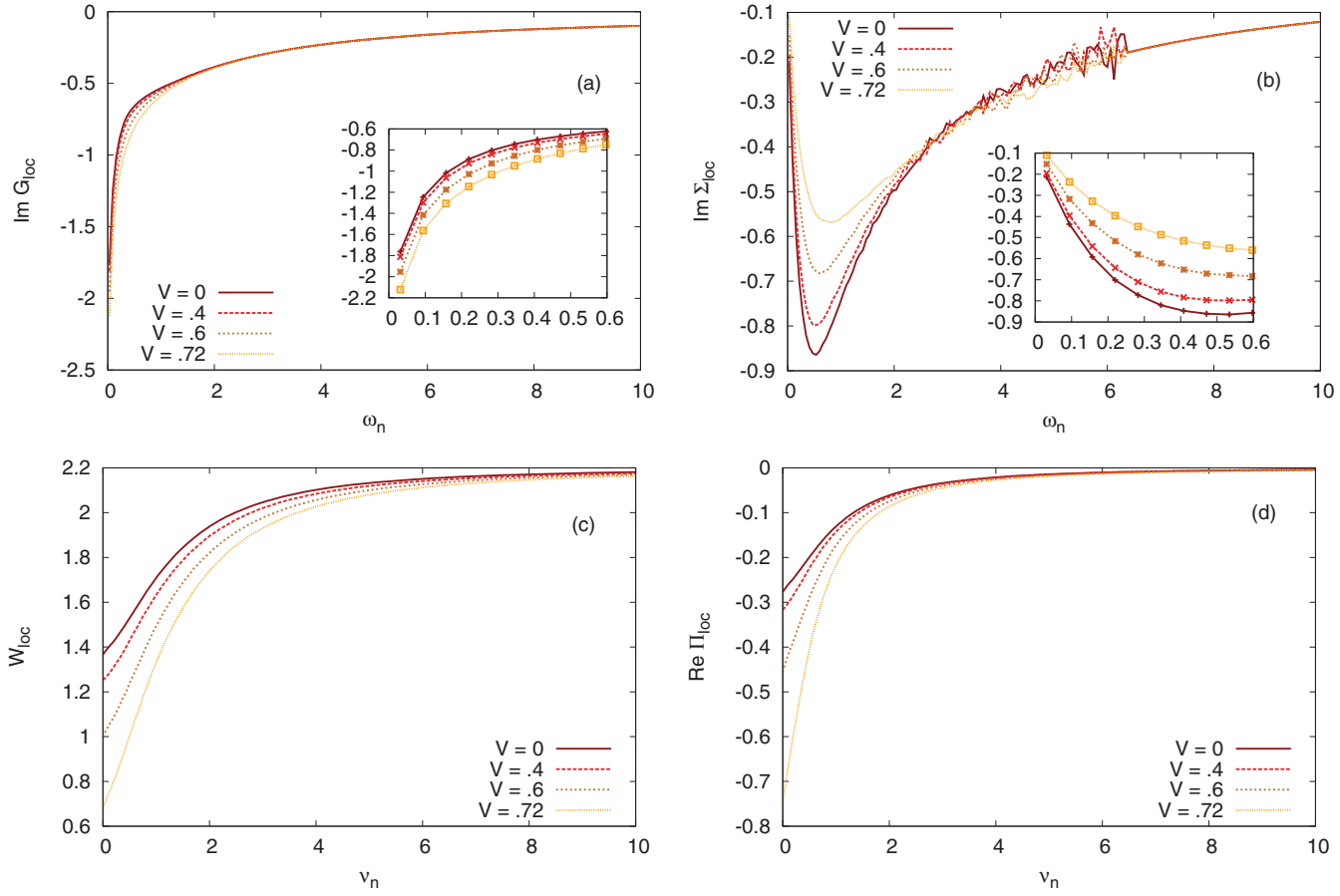

FIG. 6. (Color online) Imaginary-frequency data for the EDMFT calculations at $U = 2.2$ and indicated values of V (HS-UV scheme). (a) $\mathrm{Im}G_{\mathrm{loc}}(i\omega_n)$. (b) $\mathrm{Im}\Sigma_{\mathrm{loc}}(i\omega_n)$. (c) $\mathrm{Re}W_{\mathrm{loc}}(i\nu_n)$. (d) $\mathrm{Re}\Pi_{\mathrm{loc}}(i\nu_n)$.

slope in the critical line can be ascribed to the very nature of the two transitions at stake: one is a transition between a metal and a charge-ordered insulator, the other takes place between an incompressible Mott insulator and a charge-ordered insulator. The slope change is accompanied by a discontinuity of the V_c line at its junction with the Mott critical line: this is due to the first-order character of the Mott transition within DMFT. We note that the critical value $V_c(U)$ for $U > U_c$ is substantially larger than its naive mean field estimate. EDMFT may, however, overestimate the effect of the local interaction, so that the true value of V_c is lower.

The effect of the GW contribution to the phase diagram depends on the decoupling scheme. For HS-UV, GW does not have any influence on the phase boundaries, while in HS-V, GW substantially lowers the FL-CO phase boundary. This has the following origin: the HS-V scheme resums the diagrammatic series for V and for U separately (and treats U only to second order), whereas the HS-UV scheme resums both terms simultaneously. HS-UV is thus better poised to capture the competition between the localizing term U and the delocalizing term V. That GW in this scheme does not alter the phase boundaries should therefore come as no surprise: it merely shows that the local (EDMFT) physics alone fixes the critical value of the nonlocal interaction, and suggests that the HS-V decoupling underestimates V_c. For this reason, we will henceforth restrict most of our attention to the HS-UV scheme.

Figure 6 plots the results for $\mathrm{Im}G_{\mathrm{loc}}(i\omega_n)$, $\mathrm{Re}W_{\mathrm{loc}}(i\omega_n)$, $\mathrm{Im}\Sigma_{\mathrm{loc}}(i\omega_n)$, and $\mathrm{Re}\Pi_{\mathrm{loc}}(i\omega_n)$ corresponding to the EDMFT simulation at $U = 2.2$ and various values of V. As V grows, $|\mathrm{Im}G(i\omega_0)|$ increases and $|\Sigma_{\mathrm{loc}}(i\omega_0)|$ decreases, which indicates that the system becomes more metallic as a result of screening by V. Indeed, the screening effect can be quantified by the static values of the fully screened interaction $W(0) \equiv W_{\mathrm{loc}}(i\nu_0)$ and of the partially screened interaction $U(0) \equiv \mathcal{U}(i\nu_0)$, which are plotted in Fig. 9. The nearest-neighbor repulsion V induces a screening of the onsite Hubbard U, which becomes $U(0)$. When V increases, $W(0)$ and $U(0)$ get smaller and smaller, resulting in a more metallic behavior. For U close to U_c, the transition to the charge-ordered insulator occurs close to the value of V for which the cost of doublon formation vanishes, i.e., when $W(0) = 0$.

The last panel of Fig. 6 shows the polarization $\Pi_{\mathrm{loc}}(i\nu_n)$ (which is the local bosonic self-energy). $|\Pi_{\mathrm{loc}}(i\nu_0)|$ gets larger as one approaches the phase boundary.

B. Screening in EDMFT

1. *Screened interaction*

The off-site interactions translate into an effective retarded interaction at the level of the impurity action, as made apparent in Eq. (23). The frequency-dependent local interactions in the HS-UV formalism are now described by $\mathcal{U}(\omega)$ [or $U + \mathcal{D}(\omega)$

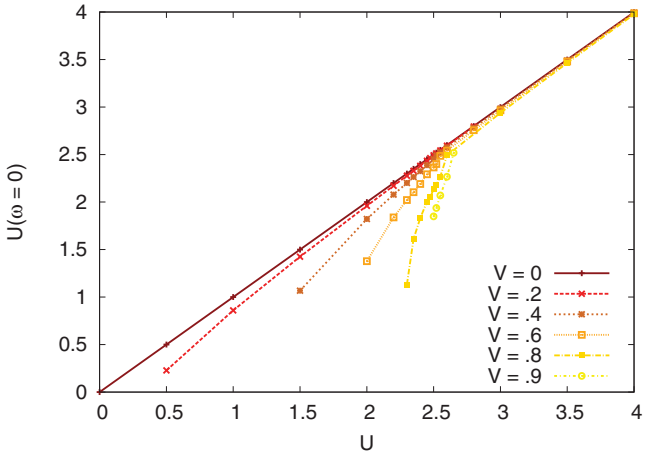

FIG. 7. (Color online) Partially screened $\mathcal{U}(\omega = 0)$ as a function of U (HS-UV scheme).

in the HS-V decoupling scheme]. They differ from the fully screened local interactions $W_{\rm loc}$ insofar as they only include nonlocal screening effects, at least in EDMFT. In particular, when the interactions become local ($V = 0$), $\mathcal{U}$ becomes static and equal to the bare interaction U, and EDMFT becomes exactly equivalent to the usual single-site DMFT. This is shown in Fig. 7, where $\mathcal{U}(\omega = 0) = U$ for $V = 0$, and explains the location of the Mott transition for $V = 0$, which coincides with that found within single-site DMFT applied to the Hubbard model. Moreover, one should also emphasize that using a partially screened interaction (i.e., screened only by nonlocal processes) to solve the impurity model, one avoids double counting of the local screening effects, which are taken into account in the DMFT calculation.

In the following, we will focus more specifically on $W_{\rm loc}$, which we have analytically continued to real frequencies using a Padé scheme.[64] The shape of $W_{\rm loc}(\omega)$ at $U = 2.2$ and various V is displayed in Fig. 8. $W_{\rm loc}(\omega)$ has the typical shape of a screened interaction: the real part features two distinct energy scales, a bare interaction $W_\infty = W_{\rm loc}(\omega \to \infty) = U$ at high energies and a screened interaction $W(0) = W_{\rm loc}(\omega = 0) < U$ at low energies, separated by a screening frequency ω_0. Its Kramers-Kronig-conjugated imaginary part has most of its spectral weight concentrated around ω_0. We note that $\mathcal{U}(\omega)$ has a very similar overall shape. Also noteworthy is the fact that $\mathrm{Re}W_{\rm loc}(\omega)$ can become negative at a nonzero frequency *before* its static value vanishes, that is, before the phase transition. This signals that charge-ordering fluctuations to charge-ordered configurations are already enhanced in the system before the phase transition occurs.

In order to characterize screening effects, we will mainly focus on the following three parameters: (i) the value of the local static screened interaction $W_{\rm loc}(0)$, (ii) the screening frequency ω_0, and (iii) the strength λ of this screening, which we will define later.

$W_{\rm loc}(0)$ is the effective fully screened interaction between two electrons on the same lattice site. Its evolution across the U-V plane for the HS-UV scheme is illustrated in Fig. 9. $W_{\rm loc}(0)$ decreases for increasing V, and drops to zero as V approaches V_c. This is intuitively easy to understand: the critical line corresponds to the locus where the cost

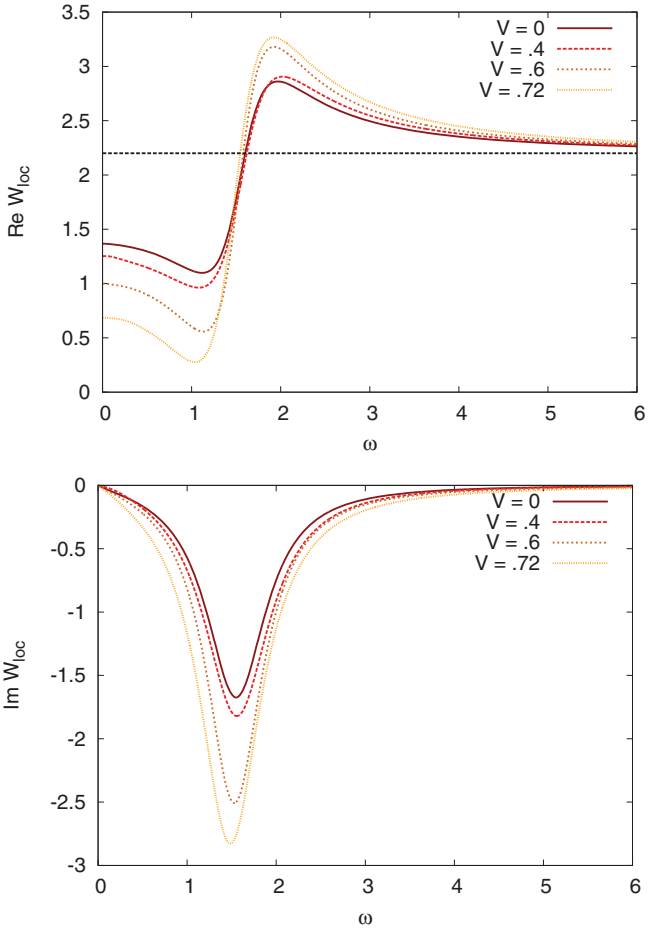

FIG. 8. (Color online) Influence of V on the effective local interaction for $U = 2.2$ (HS-UV scheme). Upper panel: $\mathrm{Re}W_{\rm loc}(\omega)$. Lower panel: $\mathrm{Im}W_{\rm loc}(\omega)$.

$W_{\rm loc}(\omega = 0)$ for the formation of doublons vanishes. The lower panel of Fig. 9 shows that the screening of the local interaction is much more efficient and gradual in the metallic phase than in the Mott insulator. In the insulating phase, screening is weak and weakly V dependent, all the way up to V_c. Let us emphasize that there are screening effects even when $V = 0$ in the metallic phase (middle panel, red curve with crosses). This shows that in a EDMFT description of the simple Hubbard model ($V = 0$), there is a screening of the static U by the *local* polarization caused by U itself, provided one uses the HS-UV decoupling scheme. In the HS-V method, the screening comes only from V, as D originates from the HS decoupling of the nearest-neighbor interaction only. The local static interactions without polarization effects are shown in Fig. 9. As expected, $\mathcal{U}(\omega = 0) > W(0)$ since the local polarization further screens the local interaction.

2. *Screening frequency*

A relevant question is in which parameter regime a model with a static screened interaction provides a reasonable approximation. A useful quantity to investigate in this context is the screening frequency ω_0, whose precise determination is a somewhat tricky task owing to the Padé procedure's inaccuracy. Instead of measuring ω_0 as the minimum of

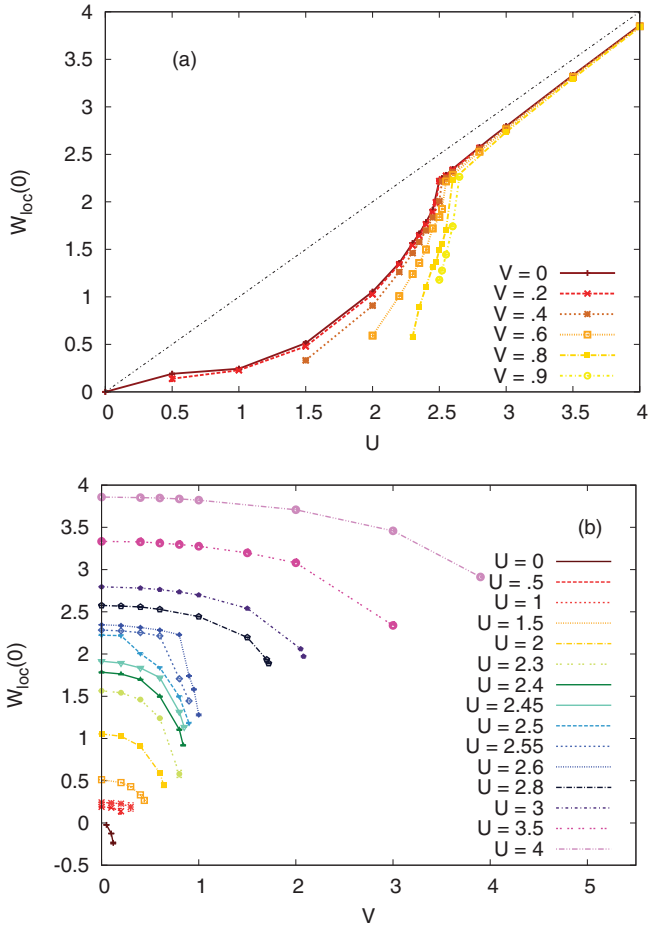

FIG. 9. (Color online) Static screened interactions in the HS-UV scheme. (a) Fully screened $W_{\rm loc}(\omega=0)$ as a function of U. (b) $W_{\rm loc}(\omega=0)$ as a function of V.

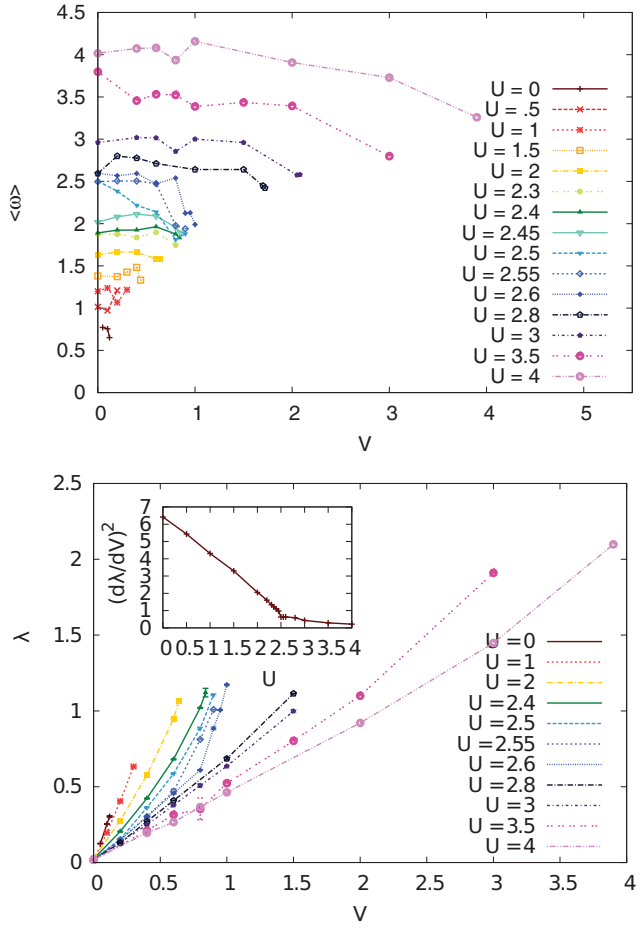

FIG. 10. (Color online) Screening parameters. Upper panel: $\langle\omega\rangle$ as a function of V. Lower panel: λ as a function of V (HS-UV scheme). Inset: $(\frac{d\lambda}{dV})^2$ as a function of U.

$\mathrm{Im}W_{\rm loc}(\omega)$, we have found it more meaningful to determine it from the first moment of $\mathrm{Im}W_{\rm loc}(\omega)$: $\omega_0 \approx \langle\omega\rangle \equiv \int_0^\infty d\omega\,\omega\,\mathrm{Im}W_{\rm loc}(\omega)/\int_0^\infty d\omega\,\mathrm{Im}W_{\rm loc}(\omega)$, whose dependence on U and V in the HS-UV scheme is presented in the upper panel of Fig. 10. This figure shows that the screening frequency is only weakly dependent on the nearest-neighbor interaction V. On the other hand, the larger the bare interaction $U = U_\infty$, the larger the screening frequency.

The U dependence of $\langle\omega\rangle$ (for $V = 0$) is discussed in Appendix D, where we also provide an interpretation of the two regimes, separated by a kink at $U = U_c$, based on the so-called linearized DMFT.[65]

3. *Electron-boson coupling*

Motivated by the Hamiltonian representation of the impurity model with dynamically screened interaction (see Appendix C), we define the strength of the screening by the parameter $\lambda \equiv \sqrt{|\int_0^\infty d\omega\,\mathrm{Im}\mathcal{U}(\omega)|}$. It follows from Eq. (C5) that $\lambda \propto \sqrt{\sum_p \lambda_p^2}$, where λ_p is the coupling of the harmonic oscillator with frequency ω_p to the charge on the impurity. Therefore, λ can be interpreted as the strength of the coupling to the charge fluctuations. Its dependence on U and V is presented in the lower panel of Fig. 10. Except in the vicinity of the phase transition to the charge-ordered phase, λ is proportional to V. The square of the proportionality constant (see inset[66]) decreases with increasing U, and exhibits two regimes separated by a kink at $U = U_c$: for $U \leqslant U_c$, $\frac{d}{dU}[(\frac{d\lambda}{dV})^2] \approx -2.2$, otherwise $\frac{d}{dU}[(\frac{d\lambda}{dV})^2] \approx -0.34$. Recalling that the effective dynamical interaction is, schematically, $\lambda^2\mathcal{D}$, where $\mathcal{D}$ is the propagator of the mediating boson (see Appendix C), one can observe that $[d\lambda/dV]^2$ is directly proportional to the effective interaction, since $\lambda \approx [d\lambda/dV]_{V=0} \cdot V$. The inset of the upper panel of Fig. 10 thus gives a direct indication of the strength of dynamical effects. In particular, it indicates once again that screening in the Mott insulator is radically different from screening in the Fermi-liquid metal.

4. *Influence of screening on spectral properties*

The screening effects coming from U and V have some impact on the local spectral function. In the weakly correlated regime ($U < U_c$), the nonlocal interactions V tend to smooth out the incoherent Hubbard bands and transfer some spectral weight to the quasiparticle peak and into the gap region between the quasiparticle peak and the Hubbard bands (Fig. 11, upper panel). This behavior is consistent with the imaginary-frequency data showing a more metallic behavior as V increases. The effects are more dramatic in the strongly

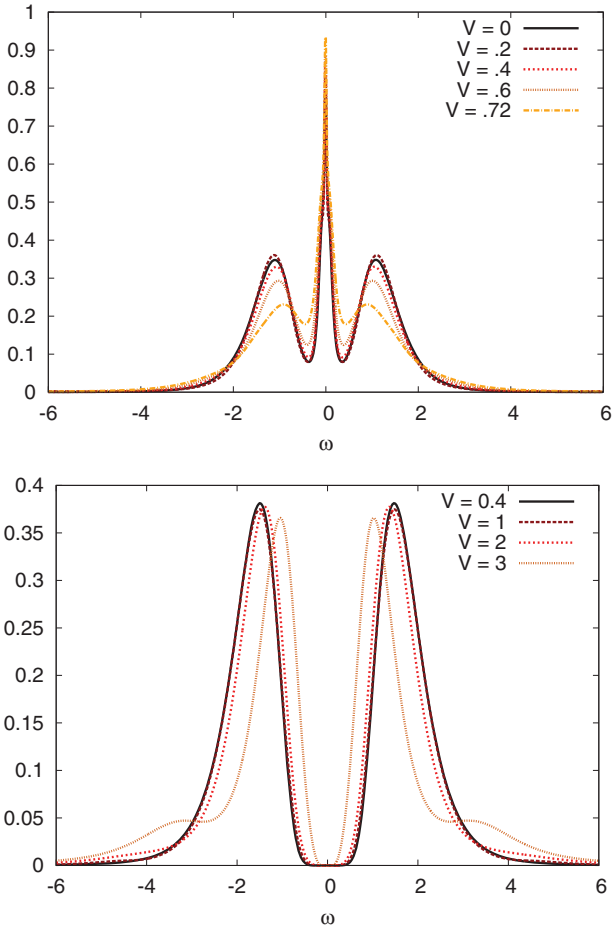

FIG. 11. (Color online) Local spectral function $A_{\rm loc}(\omega)$ (HS-UV scheme).

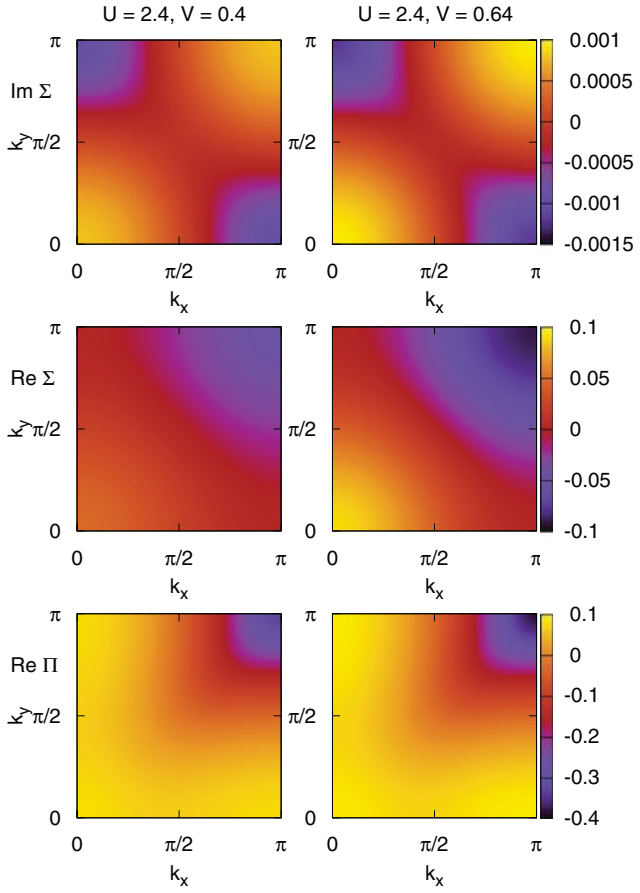

FIG. 12. (Color online) GW nonlocal contribution in the HS-UV scheme. Top: $\mathrm{Im}\Sigma^{GW}_{\rm nonloc}(k,i\omega_{n=0})$. Middle: $\mathrm{Re}\Sigma^{GW}_{\rm nonloc}(k,i\omega_{n=0})$. Bottom: $\mathrm{Re}\Pi^{GW}_{\rm nonloc}(k,i\nu_{n=0})$.

correlated regime ($U > U_c$), where one observes new features in the local spectral function, as shown in the lower panel of Fig. 11. In addition to the two Hubbard bands located at $\omega = \pm U/2$, the spectral function has two symmetric satellites at $\omega = \pm(U/2 + \omega_0)$, whose spectral weight grows with V. The position of the peaks comes from the convolution in Eq. (40) since $A_{\rm aux}$ contains spectral weight at $\pm U/2$ and B contains weight at $\pm\omega_0$.

C. Momentum dependence in GW + DMFT

1. Nonlocal self-energy

Figure 12 displays $\Sigma^{GW}_{\rm nonlocal}(k,i\omega_0)$ and $\Pi^{GW}_{\rm nonlocal}(k,i\nu_0)$ in the metallic phase near the charge-ordering transition. These quantities vanish in the limit of large dimensions and are thus neglected in the EDMFT treatment. The GW contribution to the imaginary part of the electronic self-energy Σ is negligible with respect to the local self-energy [for instance, at $U = 2$ and $V = 0.6$, $\mathrm{Im}\Sigma_{\rm loc}(i\omega_0) = -0.18$, compared to a nonlocal GW self-energy < 0.001]. This holds across the Fermi-liquid phase and the Mott insulating phase. The real part of $\Sigma^{GW}_{\rm nonlocal}$ is relatively large away from the EDMFT Fermi surface, but does not alter this Fermi surface. On the other hand, the nonlocal polarization is comparable to its local counterpart [$\Pi_{\rm loc}(i\nu_0) = -0.39$ for $U = 2$, $V = 0.6$].

This should have an impact on the phase diagram if one recalls the criterion of Eq. (42). However, the *local* observables are also modified in the self-consistent calculation, as will be described in the next section, which prevents a direct prediction of the effect of the nonlocal terms. As shown in Fig. 5, the effect of GW depends on the decoupling scheme. For the HS-UV scheme, the GW contribution has a negligible influence on the phase diagram. For the HS-V scheme, the GW contribution has a large effect on the phase boundary between the metallic phase and the charge-ordered phase. The nonlocal polarization, peaked at $k = (\pi,\pi)$, enhances nesting effects and leads to a substantially lower V_c compared to EDMFT.

2. Nonlocal polarization

Two-particle quantities such as the charge-charge correlation function or the electron energy-loss spectrum are quite strongly affected by the nonlocal GW contribution to the polarization, as discussed in Ref. 24. In particular, GW + DMFT gives insights into the nature of the collective modes in the homogeneous system, which EDMFT cannot give due to the local nature of its polarization.

Figure 13 shows results for the polarization function. We note that within single-site DMFT, one could in principle obtain a nonlocal polarization function from the momentum-dependent one-particle Green's function $G(k,\omega)$ (evaluated

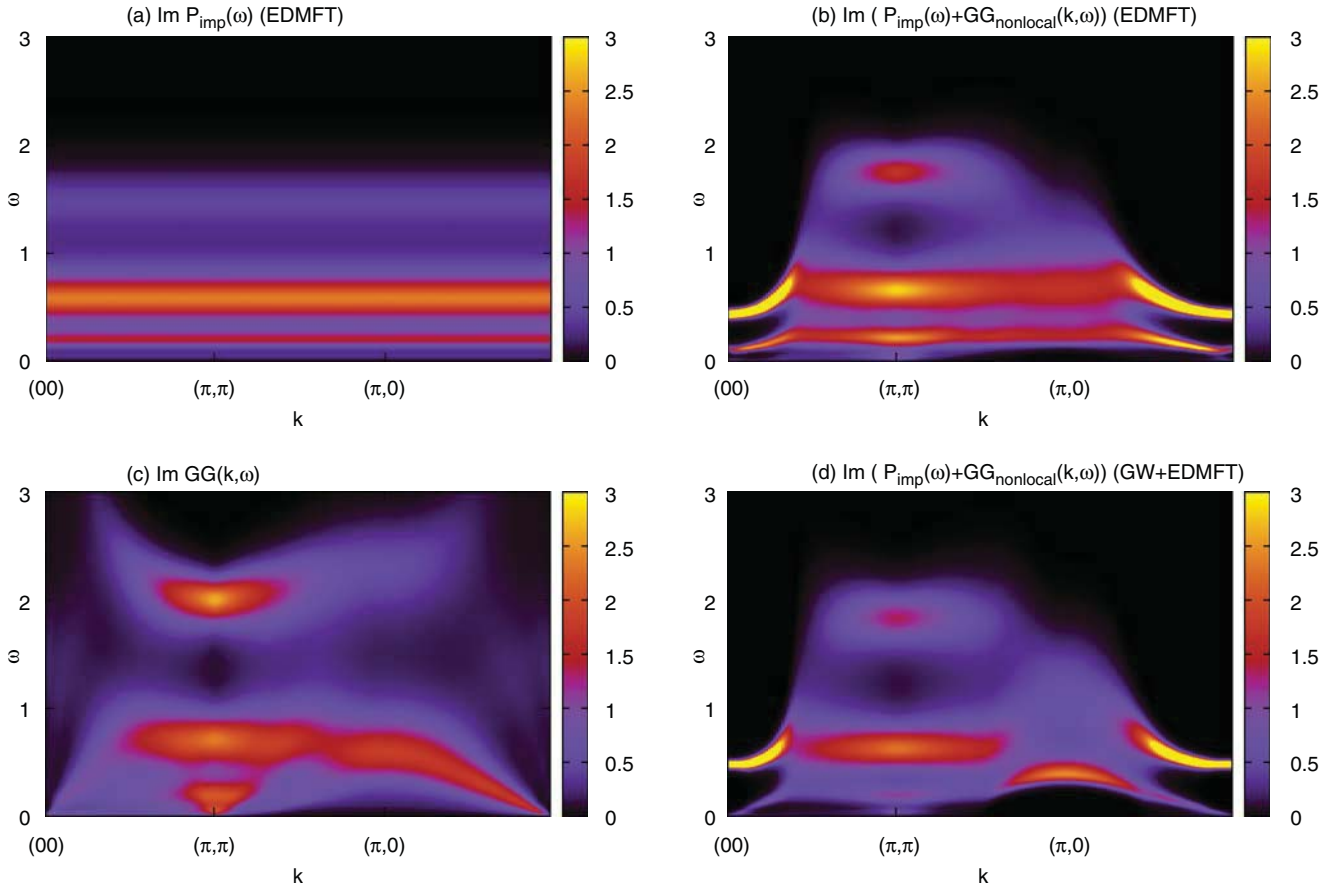

FIG. 13. (Color online) Comparison of various polarizations for $U = 1.5$, $V = 0.4$ (HS-UV scheme).

with the local EDMFT self-energy) by computing the polarization bubble GG. While this approximation to the polarization is momentum dependent, it nevertheless lacks any information about the local vertex other than through G itself. However, as was demonstrated in Ref. 24, the local vertex plays a major role when the strength U of local correlations grows. In EDMFT, on the other hand, the locality of the polarization function is assumed [see Fig. 13(a)], but the nonperturbative local vertex is taken into account since the local polarization is obtained from the nonperturbative local charge-charge correlation function. The $GW+$DMFT scheme allows one to overcome both limitations by encompassing both the local vertex (through the local part of the polarization) *and* the momentum dependence (through the nonlocal part of the bubble). In other words, conceptually, $GW+$DMFT contains more than just the bubble (through the local part of the polarization) and still yields a momentum-dependent polarization, which is more than both single-site DMFT and extended DMFT can achieve. To illustrate this point, we show in Fig. 13 the polarization bubble computed from a converged EDMFT calculation in Fig. 13(c), and the full, converged polarization of a $GW+$DMFT calculation in Fig. 13(d) (for $U = 1.5$, $V = 0.4$).

Using the output of the converged EDMFT calculation, namely, the local self-energy $\Sigma_{\rm imp}$ and the polarization $P_{\rm imp}$, one could again construct a momentum-dependent polarization in the following way: first, compute the one-particle Green's function $G(k,\omega)$ from $\Sigma_{\rm imp}$ through Dyson's equation; second, compute the bubble GG; third, combine it with $P_{\rm imp}$ to get the momentum-dependent polarization: $P(k,\omega) = P_{\rm imp}(\omega) + (GG)_{\rm nonloc}(k,\omega)$. This approach is similar to the $GW+$DMFT method with the important difference that it is not self-consistent, namely, the computed momentum-dependent polarization is not in turn used as an input to the next computational step. Even if the momentum dependence is physically important, it will not in this scheme have a consequence on the local one-particle spectra, for example. In Fig. 13, we compare this polarization [Fig. 13(b)] to the $GW+$DMFT polarization [Fig. 13(d)]. While being quite similar in certain regions of the Brillouin zone, the two functions are very different in others [above the $(\pi,0)$ point for instance]. In particular, one notices that the structure of the polarization computed on top of EDMFT, albeit momentum dependent, is very similar to the local EDMFT polarization [Fig. 13(a)] away from the $(0,0)$ point, while the $GW+$DMFT polarization shows significant deviations from it throughout the Brillouin zone.

D. Influence of the self-consistency on local observables

The self-consistency condition leads to an "adjustment" of the local quantities to the nonlocal self-energies, as shown in Fig. 14, which illustrates the convergence from EDMFT to $GW+$DMFT: GW not only adds a nonlocal contribution to the self-energy and polarization, it also induces a change in the *local* observables (see also Fig. 15).

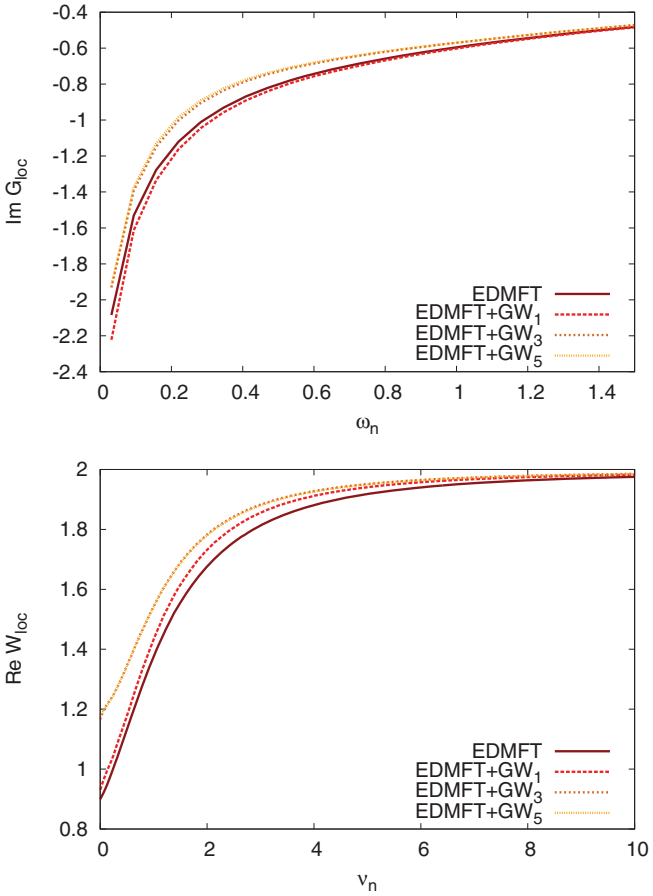

FIG. 14. (Color online) Convergence properties for $U = 2$, $V = 0.4$ (HS-UV scheme). EDMFT corresponds to the converged EDMFT result, EDMFT + GW_i denotes the observables corresponding to the ith iteration with nonlocal self-energies, with EDMFT as starting input. Upper panel: Im$G_{\rm loc}(i\omega_n)$. Lower panel: Re$W_{\rm loc}(i\nu_n)$.

The GW + DMFT local spectral function features more pronounced Hubbard bands than the EDMFT spectrum. This is a sign of increased local correlations. Inspection of the imaginary frequency data corroborates this observation: $W_{\rm loc}(\omega = 0)$ is enhanced with respect to the EDMFT result, indicating that the local interactions are stronger. Likewise, $|{\rm Im}G_{\rm loc}(i\omega_0)|$ is reduced in GW + DMFT.

These observations mean that the local quantities have become more "insulating" in character as a result of the addition of the nonlocal GW self-energy. This can be interpreted in the following way: contrary to the EDMFT case, where all the screening and correlation effects are absorbed into the local self-energy, in GW + DMFT some of these effects are now carried by the nonlocal components. Specifically, GW nonlocal self-energies carry important screening effects owing to the very nature of the GW approximation. This leads to a redistribution of the screening between local and nonlocal observables: local observables become less screened, and thus more correlated.

We note that the convergence properties depend on the observable. For example, after the first iteration, Im$G_{\rm loc}$ looks more metallic than the EDMFT result, while the converged solution is more strongly correlated. In the case of Re$W_{\rm loc}$ already the first iteration leads to an increase in the interaction.

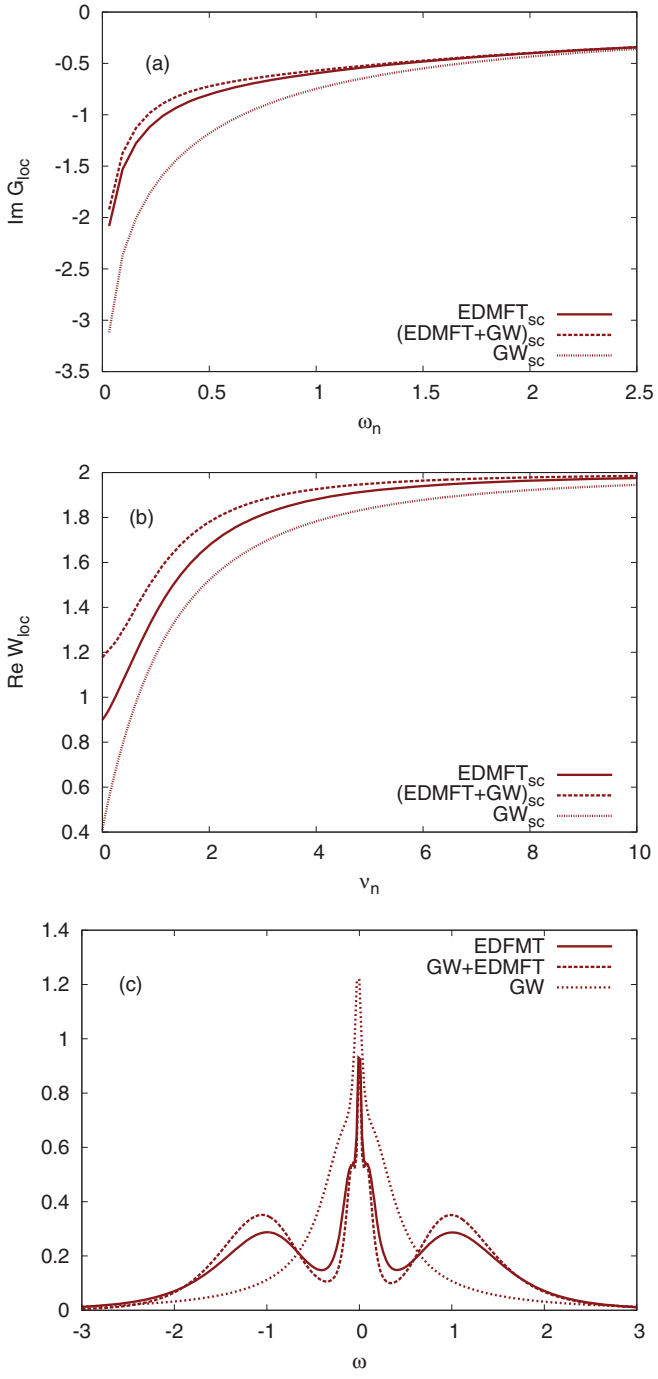

FIG. 15. (Color online) Influence of the self-consistency for $U = 2$, $V = 0.4$ (HS-UV scheme). (a) Im$G_{\rm loc}(i\omega_n)$. (b) Re$W_{\rm loc}(i\nu_n)$. (c) $A_{\rm loc}(\omega)$ (obtained from MaxEnt continuation).

In both cases, the result is clearly not converged after one iteration, which casts some doubt on the validity of "one-shot" GW + DMFT schemes.

Figure 15 shows the converged Im$G_{\rm loc}$ and Re$W_{\rm loc}$ for the three self-consistent schemes: EDMFT alone, GW + DMFT, and GW alone (with the GW + DMFT result as a starting point). As expected, GW is the most metallic in character and the corresponding spectrum does not have Hubbard bands. Interestingly, GW + DMFT is not a kind of "average" between

TABLE I. Summary of the different schemes.

	HS-V	HS-UV
Single-site DMFT	Accurate treatment of local interactions from weakly correlated limit to atomic limit. Cannot deal with long-range interactions beyond Hartree level. Local description of correlations through a local self-energy. Captures Mott transition.	
EDMFT	Accurately handles local interactions from weakly correlated limit to atomic limit. Captures Mott transition and charge-ordering transition. Deals with long-range interactions through dynamical interactions at the local level. Describes local one-particle correlations through the local self-energy. Captures local polarization processes.	Same as HS-V. Additionally, allows one to compute a fully screened interaction $W_{\mathrm{loc}}(\omega)$, screened by a nontrivial local polarization, even when $V = 0$.
GW	Accurately handles local and nonlocal (including long-ranged) interactions in the weakly correlated regime. Captures local and nonlocal polarization processes, among which nesting effects. The self-energy sums up the subset of local and nonlocal diagrams to infinite order in V, to second order in U, possibly overestimating nonlocal processes.	Same as HS-V, but treats both local and nonlocal interaction terms at the same level of approximation, i.e., to infinite order. Hence, gives better account of competition between local and nonlocal processes.
GW + DMFT	Accurate treatment of local and nonlocal (including long-ranged) interactions from weakly correlated regime to atomic limit. Captures local and nonlocal polarization processes, among which nesting effects. At a given iteration, the self-energy sums up all the local diagrams to infinite order in U and V, as well as a (RPA) subset of nonlocal diagrams to infinite order in V, to second order in U, thus overestimating nonlocal processes; in particular, underestimates the value of the critical V to the charge-ordered phase compared to HS-UV. Intersite antiferromagnetic fluctuations are not included.	Same as HS-UV, but the nonlocal diagrams treat U and V on the same footing, curing the deficiency of HS-V; in particular, gives better estimate of critical V to the charge-ordered phase.

GW and EDMFT. It exhibits stronger correlation effects than both GW and EDMFT.

E. Summary

Table I gives a general overview of the results presented above.

VII. CONCLUSIONS

We have implemented the EDMFT and GW + DMFT methods and presented an application to the single-band extended Hubbard model. In a first step, the two formalisms have been reviewed in detail: we have discussed the construction of the free-energy functional, and compared two different flavors of such functionals that have been proposed in the literature, corresponding to two distinct decouplings of the interaction term, and leading, respectively, to the GW + DMFT (Refs. 16–18) and GD + SOPT + DMFT (Refs. 14 and 15) approaches. We have presented the details of our implementation of a fully self-consistent GW + DMFT scheme based on a numerically exact continuous-time quantum Monte Carlo solver adapted for frequency-dependent local interactions. The investigation of the frequency dependence of these interactions for parameters ranging from weak to strong coupling shows that the U dependence of the local screening frequency reflects the form of the local one-particle spectrum. We have investigated the spectral properties of the extended Hubbard model within three self-consistent schemes, namely, EDMFT, GW, and GW + DMFT. The nearest-neighbor repulsion V leads, in the Mott insulator, to high-energy satellites in the local spectra.

The GW + DMFT calculations demonstrate that the nonlocal contributions to the self-energy coming from the GW diagrams are quite small in the case of the extended Hubbard model. In view of the strong momentum dependence observed in self-energies obtained from cluster DMFT calculations for the two-dimensional Hubbard model as one approaches the Mott transition,[67,68] our results confirm the importance of spin fluctuations, suggesting that further nonlocal diagrams have to be considered in order to capture the dominant fluctuations in the extended Hubbard model.

The model calculations presented in this paper can be straightforwardly extended to the multiorbital case and to additional, longer-range matrix elements of the screened interaction, paving the way for realistic first-principles material calculations.[26] It is worthwhile to note that the GW + DMFT method and its variations are a computationally cheap way of incorporating the leading vertex contribution, in the form of the EDMFT self-energy, into the description of a solid, and to introduce some spatial fluctuations through a perturbative scheme. This contrasts with methods involving an explicit computation of the vertex functions[7,9,69] whose implementation for simple model systems is already a formidable challenge.

In real materials, further degrees of freedom, stemming for example from the multiband nature and ligand orbitals, lead to a renormalization and/or frequency-dependence of the parameters in the low-energy description. Relatively weak, but nonlocal correlation effects are expected to play a dominant role in the case of extended ligand or higher-lying empty states, thus providing an additional motivation for a combination of GW and DMFT. Indeed, GW provides an accurate

and comparatively inexpensive description of the screening from "uncorrelated" bands, making the application of the $GW+$DMFT method to electronic-structure calculations for realistic solids highly promising.

ACKNOWLEDGMENTS

We acknowledge useful discussions with F. Aryasetiawan, M. Casula, A. Georges, M. Imada, Y. Nomura, A. Millis, and T. Miyake, as well as computing time on the Brutus cluster at ETH Zurich. This work was supported by the Swiss National Science Foundation (Grants No. PP0022_118866, No. 200021_140648, and through NCCR MANEP), DFG FOR 1346, and by the French ANR under projects CORRELMAT and SURMOTT, GENCI/IDRIS Orsay under project 1393. The Monte-Carlo scheduler uses the ALPS library.[70]

APPENDIX A: EXTENDED HUBBARD MODELS FROM FIRST PRINCIPLES

The Hamiltonian H of the extended Hubbard model is supposed to describe the low-energy physics of correlated materials. H can be regarded as an effective Hamiltonian resulting from a "downfolding procedure," based on some localized Wannier basis. The downfolding procedure is akin to a renormalization group transformation which, starting from all the bands resulting from a LDA calculation, produces an effective model for the bands in a low-energy window by integrating out the remaining bands. In this process, the bare Coulomb interaction $v(r,r')=4\pi e^2/|r-r'|$ is transformed into a frequency-dependent partially screened interaction $W_r(r,r',\omega)$,[71–73] which acts in the low-energy subspace. In principle, W_r is computed as $W_r=v(1-vP_r)^{-1}$, where P_r is the polarization obtained when transitions within the effective model are removed. The matrix elements of this interaction in the Wannier basis are

$$V_{ijkl}(\omega)=\int d^3r\, d^3r' \phi_i^*(r)\phi_j^*(r')W_r(r,r',\omega)\phi_k(r)\phi_l(r'), \tag{A1}$$

where ϕ_i denotes a Wannier orbital centered at site i.

Model (1) involves three approximations on the above matrix elements: (i) the frequency dependence of $V_{ijkl}(\omega)$ is neglected: $V_{ijkl}\equiv V_{ijkl}(\omega=0)$, (ii) the interaction is restricted to density-density terms $V_{ijkl}=V_{ijij}\delta_{ik}\delta_{jl}\equiv V_{ij}$, and (iii) only the onsite matrix element $U\equiv V_{ii}$ and the nearest-neighbor matrix element $V\equiv V_{ij}$ (with i and j nearest neighbors) are retained. The last assumption is valid only if $W_r(r-r',\omega=0)$ decays rapidly in space.[74] The neglected non-site-diagonal parts of the electron-electron interactions such as, for instance, the bond-charge-bond-charge matrix elements $W\equiv V_{ijji}$, are believed to be small in usual solids.[75]

We also mention that a "locally unscreened cRPA" approach has been recently implemented.[76,77] It is geared at a direct construction of an impurity Hubbard interaction, akin to the one resulting from $GW+$DMFT, but computed from a single-shot RPA calculation.

APPENDIX B: DERIVATION OF THE SINGLE-SITE EDMFT ACTION USING THE CAVITY METHOD

In the following, we use the cavity method[2] to derive the EDMFT action (22) and the EDMFT self-consistency equations which fix $\mathcal{G}$ and $\mathcal{U}$. To this end, let us focus on a given site (denoted by the index 0) and split the lattice action [Eq. (8)] into three parts: $S=S_0+S^{(0)}+\Delta S$ where S_0 denotes the action of the site 0, $S^{(0)}$ the action of the lattice with site 0 removed (the lattice with a "cavity" at site 0), and ΔS the remaining part:

$$S_0=\int_0^\beta d\tau\Big\{\sum_\sigma c_{0\sigma}^*\left(\partial_\tau-\mu\right)c_{0\sigma}+i\phi_0 n_0 + \frac{1}{2}\phi_0[v^{-1}]_{00}\phi_0\Big\}, \tag{B1}$$

$$\Delta S=\int_0^\beta d\tau\Big\{-\sum_{i\neq 0,\sigma} t_{i0}(c_{0\sigma}^* c_{i\sigma}+c_{i\sigma}^* c_{0\sigma}) + \sum_{i\neq 0}\phi_i[v^{-1}]_{i0}\phi_0\Big\}, \tag{B2}$$

$$S^{(0)}=\int_0^\beta d\tau\Big\{\sum_{ij\neq 0,\sigma} c_{i\sigma}^*(\partial_\tau-\mu-t_{ij})c_{j\sigma} + \frac{1}{2}\sum_{ij,\neq 0}\phi_i[v^{-1}]_{ij}\phi_j+i\sum_{i\neq 0}\phi_i n_i\Big\}. \tag{B3}$$

Defining $\eta_{i\sigma}\equiv t_{i0}c_{0\sigma}$ and $j_i\equiv[v^{-1}]_{i0}\phi_0$, we can write $\Delta S=\int_0^\beta d\tau\{-\sum_{i\neq 0,\sigma}(\eta_i^* c_{i\sigma}+c_{i\sigma}^*\eta_i)+\sum_{i\neq 0}j_i\phi_i\}$, such that $\eta_{i\sigma}$ and j_i can be regarded as sources of correlation functions for the effective action of the site 0, defined by $e^{-S_{\rm eff}[c_0^*,c_0,\phi_0]}/Z_{\rm eff}\equiv\int\mathcal{D}_{i\neq 0}[c_i^*,c_i,\phi_i]e^{-(S_0+S^{(0)}+\Delta S)}/Z$. We can express the action as $S_{\rm eff}=S_0-\Omega[\eta_i^*,\eta_i,j_i]+\text{const}$, where $\Omega[\eta_i^*,\eta_i,j_i]\equiv\ln\int\mathcal{D}_{i\neq 0}[c_i^*,c_i,\phi_i]e^{-(S^{(0)}+\Delta S)}$ is the generating functional of connected correlation functions of the cavity,[47]

$$G^{(0)}_{i_1\ldots i_n j_n\ldots j_1}(\tau_1\ldots\tau_n,\tau_1'\ldots\tau_n') = (-1)^n\frac{\delta^{2n}\Omega}{\delta\eta^*_{i_1}(\tau_1)\ldots\delta\eta^*_{i_n}(\tau_n)\delta\eta_{j_n}(\tau_n')\ldots\delta\eta_{j_1}(\tau_1')}, \tag{B4}$$

$$W^{(0)}_{i_1\ldots i_n j_n\ldots j_1}(\tau_1\ldots\tau_n,\tau_1'\ldots\tau_n') = \frac{\delta^{2n}\Omega}{\delta j_{i_1}(\tau_1)\ldots\delta j_{i_n}(\tau_n)\delta j_{j_n}(\tau_n')\ldots\delta j_{j_1}(\tau_1')}. \tag{B5}$$

An explicit expression for Ω is thus

$$\begin{aligned}\Omega[\eta_i^*,\eta_i,j_i]=&\sum_{n=1}^\infty\sum_{i_1\ldots i_n,j_1\ldots j_n}\int d\tau_1\ldots d\tau_n'\eta^*_{i_1}(\tau_1)\ldots\eta_{j_1}(\tau_n')\\ &\times(-1)^n G^{(0)}_{i_1\ldots i_n j_n\ldots j_1}(\tau_1\ldots\tau_n')\\ &+\sum_{n=1}^\infty\sum_{i_1\ldots i_n,j_1\ldots j_n}\int d\tau_1\ldots d\tau_n' j_{i_1}(\tau_1)\ldots j_{j_n}(\tau_n')\\ &\times W^{(0)}_{i_1\ldots i_n j_n\ldots j_1}(\tau_1\ldots\tau_n').\end{aligned} \tag{B6}$$

The DMFT approximates Ω by its infinite-dimensional limit. In this limit, the hopping t between sites must be scaled as $t/\sqrt{z}$ (with $z=2d$) in order to keep a finite kinetic energy, while V must be scaled as V/z in order to keep

the Hartree energy corresponding to the nearest-neighbor interaction finite.[46] As a consequence of taking this limit, all terms of order $n > 1$ in Eq. (B6) vanish, so that $\Omega^{\mathrm{DMFT}} = \int d\tau\, d\tau' c_0^*(\tau)\big(-\sum_{ij} t_{i0}t_{j0}G^{(0)}_{ij}(\tau-\tau')\big)c_0(\tau') + \int d\tau\, d\tau' \phi_0(\tau)\big(\sum_{ij} v_{i0}^{-1}v_{j0}^{-1}W^{(0)}_{ij}(\tau-\tau')\big)\phi_0(\tau')$. We thus arrive at the DMFT effective action of Eq. (21) (where we have dropped the index 0 in order to simplify the notation) with

$$\mathcal{G}^{-1}(i\omega_n) \equiv i\omega_n + \mu - \sum_{ij} t_{i0}t_{j0}G^{(0)}_{ij}(i\omega_n), \tag{B7}$$

$$\mathcal{U}^{-1}(i\nu_n) \equiv v_{00}^{-1} - \sum_{ij} v_{i0}^{-1}v_{j0}^{-1}W^{(0)}_{ij}(i\nu_n). \tag{B8}$$

Furthermore, in the limit of infinite dimensions, the cavity Green's function is related to the lattice Green's function through $G^{(0)}_{ij} = G_{ij} - G_{i0}G_{0j}/G_{00}$ and $W^{(0)}_{ij} = W_{ij} - W_{i0}W_{0j}/W_{00}$, which is shown by considering the paths contributing to G_{ij} (W_{ij}) and not to $G^{(0)}_{ij}$ ($W^{(0)}_{ij}$) (see Ref. 2 for more details). This allows us to write $\sum_{ij} t_{i0}t_{j0}G^{(0)}_{ij}$, after Fourier transformation, as

$$\sum_k \epsilon_k^2 G_k(i\omega_n) - \left(\sum_k \epsilon_k G_k(i\omega_n)\right)^2 \Big/ \sum_k G_k(i\omega_n). \tag{B9}$$

At this point, a second approximation is made: the self-energies are assumed to be k-independent, namely, $\Sigma(k,i\omega) \approx \Sigma_{\mathrm{loc}}(i\omega)$ and $\Pi(k,i\nu) \approx \Pi_{\mathrm{loc}}(i\nu)$. This also becomes exact in the $d \to \infty$ limit.[78] As a consequence, we can define the densities of states $\rho(\epsilon) = \sum_k \delta(\epsilon - \epsilon_k)$ and $\rho'(\epsilon) = \sum_k \delta(\epsilon - v_k^{-1})$, which allows us to rewrite (B9) as

$$\int \frac{d\epsilon\, \rho(\epsilon)\epsilon^2}{\zeta - \epsilon} - \left(\int \frac{d\epsilon\, \rho(\epsilon)\epsilon}{\zeta - \epsilon}\right)^2 \Big/ \int \frac{d\epsilon\, \rho(\epsilon)}{\zeta - \epsilon}, \tag{B10}$$

where $\zeta \equiv i\omega_n + \mu - \Sigma_{\mathrm{loc}}(i\omega_n)$. The same expression holds for the screened interaction, with $\rho \to \rho'$ and $\zeta \to \zeta' = [v^{-1}]_{00} - \Pi_{\mathrm{loc}}(i\nu_n)$ [as can be seen by comparing Eqs. (B7) and (B8)].

Using the following identities for Hilbert transforms,

$$\int_{-\infty}^{\infty} \frac{d\epsilon\rho(\epsilon)\epsilon^2}{\zeta - \epsilon} = \zeta \int_{-\infty}^{\infty} \frac{d\epsilon\rho(\epsilon)\epsilon}{\zeta - \epsilon}, \tag{B11}$$

$$\int_{-\infty}^{\infty} \frac{d\epsilon\rho(\epsilon)\epsilon}{\zeta - \epsilon} = -1 + \zeta \int_{-\infty}^{\infty} \frac{d\epsilon\rho(\epsilon)}{\zeta - \epsilon}, \tag{B12}$$

we obtain the self-consistency relations (25) and (26).

Equations (21), (25), and (26) form a closed set of equations: $S^{\mathrm{DMFT}}_{\mathrm{eff}}$, once solved, yields Σ_{loc} and Π_{loc}, which gives updated $\mathcal{G}$ and $\mathcal{U}$ which can in turn be used to solve the effective local problem again until convergence is reached.

APPENDIX C: HAMILTONIAN FORMULATION OF THE IMPURITY PROBLEM

Some properties of action (24) are more easily understood in terms of its Hamiltonian representation. The first two terms correspond to an Anderson impurity model

$$H_{\mathrm{AIM}} = \sum_p \varepsilon_p a_p^\dagger a_p + \sum_p \left(V_p^\sigma a_{p\sigma}^\dagger c_\sigma + \mathrm{H.c.}\right) + Un_\uparrow n_\downarrow - \mu n, \tag{C1}$$

describing an impurity (c, $c^\dagger$) coupled to a bath of noninteracting fermionic levels (a_p, $a_p^\dagger$, energy ε_p). Here, $n_\sigma = c_\sigma^\dagger c_\sigma$ and $n = n_\uparrow + n_\downarrow$. The connection between Eqs. (24) and (C1) is given by $\mathcal{G}^{-1}(i\omega_m) = i\omega_m + \mu - \Delta(i\omega_m)$ and the hybridization function $\Delta(i\omega_m) = \sum_p \frac{|V_p^\sigma|^2}{i\omega_m - \varepsilon_p}$. On the other hand, the retarded effective interaction can be generated by coupling the impurity to a bath of bosonic modes described by the Hamiltonian

$$H_{\mathrm{boson}} = \sum_p \omega_p b_p^\dagger b_p + \sum_p \frac{\lambda_p}{\sqrt{2}} n(b_p + b_p^\dagger) = \sum_p \frac{\omega_p}{2}\left(\phi_p^2 + \Pi_p^2\right) + \sum_p \lambda_p n_0 \phi_p, \tag{C2}$$

with $\phi_p \equiv \frac{1}{\sqrt{2}}(b_p + b_p^\dagger)$ and $\Pi_p \equiv \frac{1}{i\sqrt{2}}(b_p - b_p^\dagger)$.

Using the identity $\Pi_p^2(\tau) = -[\partial_\tau \phi_p(\tau)]^2/\omega_p^2$, this can be written in an action formulation as

$$S_{\mathrm{boson}} = \frac{1}{\beta}\sum_{m,p} \phi_p(i\nu_m)\left(\frac{-(i\nu_m)^2 + \omega_p^2}{2\omega_p}\right)\phi_p(-i\nu_m) + \lambda_p \phi_p(i\nu_m) n(-i\nu_m). \tag{C3}$$

Integrating out the bosonic degrees of freedom leads to

$$S_{\mathrm{boson}} = \frac{1}{\beta}\sum_m n(i\nu_m)\left\{-\sum_p \lambda_p^2 \frac{2\omega_p}{(i\nu_m)^2 - \omega_p^2}\right\} n(-i\nu_m). \tag{C4}$$

Defining $\mathcal{D}(i\nu_m) = \int \frac{d\omega}{\pi} \mathrm{Im}\mathcal{D}(\omega)\frac{2\omega}{(i\nu_m)^2 - \omega^2}$ with

$$\mathrm{Im}\mathcal{D}(\omega) \equiv -\pi \sum_p \lambda_p^2 \delta(\omega - \omega_p) \tag{C5}$$

and Fourier transforming $\mathcal{D}(i\nu_n)$ yields the retarded interaction in Eq. (24).

The retarded interaction may thus be regarded as stemming from the coupling to a bath of harmonic oscillators labeled by the index p, with frequency ω_p and coupling strength λ_p (as already emphasized in Ref. 11). The effective interaction mediated by these auxiliary degrees of freedom is proportional to the squared coupling strength λ_p^2 times the free-phonon Green's function[79] $D_p^0(i\nu_n) \equiv -\int_0^\beta d\tau e^{i\tau\nu_n}\langle\phi_p(\tau)\phi_p(0)\rangle = \frac{2\omega_p}{(i\nu_n)^2 - \omega_p^2}$. Note that in complete analogy to the fermionic hybridization function $\Delta(\omega)$, the frequency-dependent interaction $\mathcal{D}(\omega)$ is determined self-consistently.

APPENDIX D: SCREENING FREQUENCY FROM LINEARIZED DMFT

The U-dependence of the screening frequency may be traced back to the form of the one-particle local spectrum. As can be seen from Eq. (39), for $V = 0$,[80] the frequency dependence of W_{loc} (and thus the value of ω_0) is inherited from the charge-charge correlation function χ_{loc}. An analytical estimate for the poles of this function can be calculated by means of a simple approximation named linearized DMFT.[65] In this method, the impurity problem is approximated by the coupling of the correlated impurity to a *single* uncorrelated bath level describing the hybridization of the impurity to the

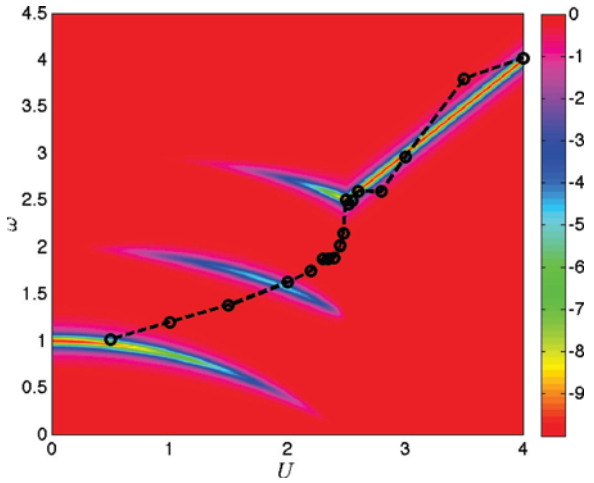

FIG. 16. (Color online) $\mathrm{Im}\chi_{\mathrm{loc}}^{l\text{-DMFT}}$ in the (ω,U) plane for $V=0$. The poles have been artificially broadened by an imaginary factor $\eta=0.01$. Black line: EDMFT result for $\langle\omega\rangle$ as a function of U (for $V=0$).

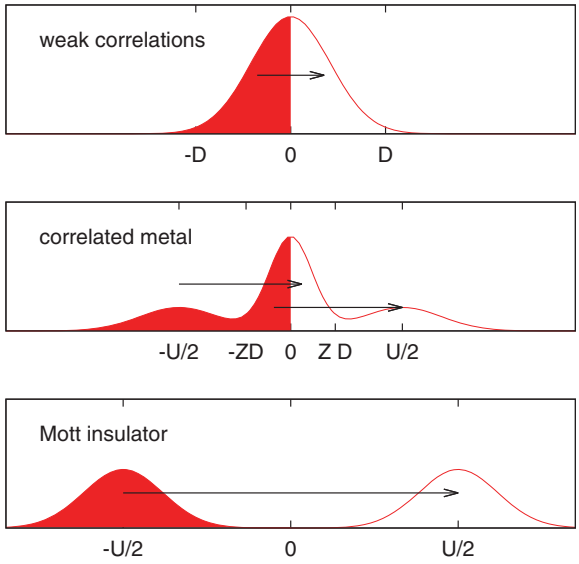

FIG. 17. (Color online) Sketch of transitions in generic spectra for the Hubbard model at various interaction strengths.

lattice degrees of freedom. This simplified version of the impurity problem allows for the explicit calculation of the local Green's function[81]:

$$G_{\mathrm{loc}}^{l\text{-DMFT}}(\omega)=\sum_{i=1}^{2}a_i\left\{\frac{1}{\omega-\bar{\epsilon}_i}+\frac{1}{\omega+\bar{\epsilon}_i}\right\} \tag{D1}$$

with

$$\bar{\epsilon}_{1,2}=\frac{1}{4}\left(\sqrt{U^2+64V_{\mathrm{hyb}}^2}\mp\sqrt{U^2+16V_{\mathrm{hyb}}^2}\right), \tag{D2}$$

$$a_1=\frac{1}{4}\left(1-\frac{U^2-32V_{\mathrm{hyb}}^2}{\sqrt{U^2+64V_{\mathrm{hyb}}^2}\sqrt{U^2+16V_{\mathrm{hyb}}^2}}\right), \tag{D3}$$

as well as $a_2=\frac{1}{2}-a_1$. The hybridization strength's dependence on U is given by $V_{\mathrm{hyb}}=t\sqrt{z}\sqrt{1-U^2/U_c^2}$ (see Ref. 65 for details). U_c denotes the critical U for the Mott transition. In the estimate below, we will use the value computed within EDMFT, $U_c=2.5$.

In the absence of vertex corrections, the corresponding charge-charge correlation function can be computed as $\chi_{\mathrm{loc}}=-2G_{\mathrm{loc}}G_{\mathrm{loc}}$, leading to the expression

$$\chi_{\mathrm{loc}}(\omega)=-2\left\{\frac{2a_1^2\epsilon_1}{\omega^2-\epsilon_1^2}+\frac{2a_2^2\epsilon_2}{\omega^2-\epsilon_2^2}+\frac{4a_1a_2\epsilon_3}{\omega^2-\epsilon_3^2}\right\}. \tag{D4}$$

The six (3×2) poles are defined as $\epsilon_1=2\bar{\epsilon}_1$, $\epsilon_2=2\bar{\epsilon}_2$, and $\epsilon_3=\bar{\epsilon}_1+\bar{\epsilon}_2$.

These poles, displayed in Fig. 16, correspond to the transitions allowed in the various correlation regimes, namely, in the low-correlation limit, only transitions within the quasiparticle peak are possible (see Fig. 17). As correlations increase, the appearance of Hubbard bands enable additional transitions from the lower Hubbard band to the unoccupied states of the quasiparticle peak, and from the occupied states of the quasiparticle peak to the upper Hubbard band. In the strong correlation regime, finally, the only possible transitions are those between the lower and the upper Hubbard bands.

[1] F. C. Zhang and T. M. Rice, Phys. Rev. B **37**, 3759 (1988).
[2] A. Georges, G. Kotliar, W. Krauth, and M. J. Rozenberg, Rev. Mod. Phys. **68**, 13 (1996).
[3] G. Kotliar and D. Vollhardt, Phys. Today **57**(3), 53 (2004).
[4] A. I. Lichtenstein and M. I. Katsnelson, Phys. Rev. B **62**, R9283 (2000).
[5] G. Kotliar, S. Y. Savrasov, G. Pálsson, and G. Biroli, Phys. Rev. Lett. **87**, 186401 (2001).
[6] M. H. Hettler, A. N. Tahvildar-Zadeh, M. Jarrell, T. Pruschke, and H. R. Krishnamurthy, Phys. Rev. B **58**, R7475 (1998).
[7] A. N. Rubtsov, M. I. Katsnelson, and A. I. Lichtenstein, Phys. Rev. B **77**, 033101 (2008).
[8] A. Rubtsov, M. Katsnelson, and A. Lichtenstein, Ann. Phys. (NY) **327**, 1320 (2012).
[9] A. Toschi, A. A. Katanin, and K. Held, Phys. Rev. B **75**, 045118 (2007).
[10] E. Kuchinskii, I. Nekrasov, and M. Sadovskii, JETP Lett. **82**, 198 (2005) [Pis'ma Zh. Éksp. Teor. Fiz. **82**, 217 (2005)].
[11] Q. Si and J. L. Smith, Phys. Rev. Lett. **77**, 3391 (1996).
[12] A. M. Sengupta and A. Georges, Phys. Rev. B **52**, 10295 (1995).
[13] H. Kajueter, Ph.D. thesis, Rutgers University, New Brunswick, 1996.
[14] P. Sun and G. Kotliar, Phys. Rev. B **66**, 085120 (2002).
[15] P. Sun and G. Kotliar, Phys. Rev. Lett. **92**, 196402 (2004).
[16] S. Biermann, F. Aryasetiawan, and A. Georges, Phys. Rev. Lett. **90**, 086402 (2003).

[17]F. Aryasetiawan, S. Biermann, and A. Georges, *Proceedings of the Conference on Coincidence Studies of Surfaces, Thin Films and Nanostructures, Ringberg castle, September 2003*, edited by J. Berakdar and J. Kirschner (Wiley-VCH Verlag GmbH & Co. KGaA, Weinheim, 2004), arXiv:cond-mat/0401626.

[18]S. Biermann, F. Aryasetiawan, and A. Georges, *Physics of Spin in Solids: Materials, Methods, and Applications* (Kluwer Academic, Dordrecht, 2004), pp. 43–65, arXiv:cond-mat/0401653.

[19]M. Casula, A. Rubtsov, and S. Biermann, Phys. Rev. B **85**, 035115 (2012).

[20]P. Werner and A. J. Millis, Phys. Rev. Lett. **99**, 146404 (2007).

[21]P. Werner and A. J. Millis, Phys. Rev. Lett. **104**, 146401 (2010).

[22]P. Werner, M. Casula, T. Miyake, F. Aryasetiawan, A. J. Millis, and S. Biermann, Nat. Phys. **8**, 331 (2012).

[23]M. Casula, P. Werner, L. Vaugier, F. Aryasetiawan, A. J. Millis, and S. Biermann, Phys. Rev. Lett. **109**, 126408 (2012).

[24]T. Ayral, P. Werner, and S. Biermann, Phys. Rev. Lett. **109**, 226401 (2012).

[25]J. M. Tomczak, M. Casula, T. Miyake, F. Aryasetiawan, and S. Biermann, Europhys. Lett. **100**, 67001 (2012).

[26]P. Hansmann, T. Ayral, L. Vaugier, P. Werner, and S. Biermann, arXiv:1301.4325.

[27]P. Werner, A. Comanac, L. de' Medici, M. Troyer, and A. J. Millis, Phys. Rev. Lett. **97**, 076405 (2006).

[28]A. N. Rubtsov, V. V. Savkin, and A. I. Lichtenstein, Phys. Rev. B **72**, 035122 (2005).

[29]C. Almbladh, U. von Barth, and R. van Leeuwen, Int. J. Mod. Phys. B **13**, 535 (1999).

[30]R. Chitra and G. Kotliar, Phys. Rev. B **63**, 115110 (2001).

[31]M. C. Gutzwiller, Phys. Rev. Lett. **10**, 159 (1963).

[32]J. Hubbard, Proc. R. Soc. London, Ser. A **276**, 238 (1963).

[33]J. Kanamori, Prog. Theor. Phys. **30**, 275 (1963).

[34]S. V. Vonsovsky and M. I. Katsnelson, J. Phys. C: Solid State Phys. **12**, 2043 (1979).

[35]R. A. Bari, Phys. Rev. B **3**, 2662 (1971).

[36]U. Wolff, Nucl. Phys. B **225**, 391 (1983).

[37]X.-Z. Yan, Phys. Rev. B **48**, 7140 (1993).

[38]Y. Zhang and J. Callaway, Phys. Rev. B **39**, 9397 (1989).

[39]P. G. J. van Dongen, Phys. Rev. Lett. **67**, 757 (1991).

[40]P. G. J. van Dongen, Phys. Rev. B **50**, 14016 (1994).

[41]P. G. J. van Dongen, Phys. Rev. Lett. **74**, 182 (1995).

[42]M. Aichhorn, H. G. Evertz, W. von der Linden, and M. Potthoff, Phys. Rev. B **70**, 235107 (2004).

[43]B. Davoudi and A.-M. S. Tremblay, Phys. Rev. B **76**, 085115 (2007).

[44]R. Pietig, R. Bulla, and S. Blawid, Phys. Rev. Lett. **82**, 4046 (1999).

[45]W. Metzner and D. Vollhardt, Phys. Rev. Lett. **62**, 324 (1989).

[46]E. Müller-Hartmann, Z. Phys. B **74**, 507 (1989).

[47]J. W. Negele and H. Orland, *Quantum Many-Particle Systems* (Westview Press, Boulder, CO, 1988).

[48]W. Kohn, Rev. Mod. Phys. **71**, 1253 (1999).

[49]J. Hubbard, Phys. Rev. Lett. **3**, 77 (1959).

[50]G. Baym, Phys. Rev. **127**, 1391 (1962).

[51]J. M. Luttinger and J. C. Ward, Phys. Rev. **118**, 1417 (1960).

[52]G. Baym and L. P. Kadanoff, Phys. Rev. **124**, 287 (1961).

[53]L. Hedin, Phys. Rev. **139**, A796 (1965).

[54]F. Aryasetiawan and O. Gunnarsson, Rep. Prog. Phys. **61**, 237 (1998).

[55]G. Onida, L. Reining, and A. Rubio, Rev. Mod. Phys. **74**, 601 (2002).

[56]M. Shishkin, M. Marsman, and G. Kresse, Phys. Rev. Lett. **99**, 246403 (2007).

[57]H. Jiang, R. I. Gomez-Abal, P. Rinke, and M. Scheffler, Phys. Rev. Lett. **102**, 126403 (2009).

[58]We do not enter here into a discussion of different levels of (partial or full) self-consistency, nor into a description of the quasiparticle self-consistent GW scheme by Kotani and Schilfgaarde (Ref. 59). See, however, the benchmark calculations in Ref. 24.

[59]T. Kotani, M. van Schilfgaarde, and S. V. Faleev, Phys. Rev. B **76**, 165106 (2007).

[60]A. Abrikosov, L. Gor'kov, and I. Dzyaloshinski, *Methods of Quantum Field Theory in Statistical Physics*, 2nd ed. (Pergamon, New York, 1965).

[61]The formula is written here in imaginary-time space.

[62]M. Jarrell and J. Gubernatis, Phys. Rep. **269**, 133 (1996), ISSN 0370-1573.

[63]S. Florens, Ph.D. thesis, Université Paris 6, Paris, 2003.

[64]H. J. Vidberg and J. W. Serene, J. Low Temp. Phys. **29**, 179 (1977).

[65]M. Potthoff, Phys. Rev. B **64**, 165114 (2001).

[66]The slope at origin of $\lambda(V)$ has been used to compute $[d\lambda/dV]_{V=0}$.

[67]P. Werner, E. Gull, O. Parcollet, and A. J. Millis, Phys. Rev. B **80**, 045120 (2009).

[68]E. Gull, O. Parcollet, P. Werner, and A. J. Millis, Phys. Rev. B **80**, 245102 (2009).

[69]G. Rohringer, A. Valli, and A. Toschi, Phys. Rev. B **86**, 125114 (2012).

[70]B. Bauer, L. D. Carr, H. G. Evertz, A. Feiguin, J. Freire, S. Fuchs, L. Gamper, J. Gukelberger, E. Gull, S. Guertler *et al.* , J. Stat. Mech.: Theor. Exp. (2011) P05001.

[71]F. Aryasetiawan, M. Imada, A. Georges, G. Kotliar, S. Biermann, and A. I. Lichtenstein, Phys. Rev. B **70**, 195104 (2004).

[72]T. Miyake and F. Aryasetiawan, Phys. Rev. B **77**, 085122 (2008).

[73]L. Vaugier, H. Jiang, and S. Biermann, Phys. Rev. B **86**, 165105 (2012).

[74]This assumption is not necessarily valid if low-energy metallic screening is due to particle-hole excitations within the low-energy window itself. However, extending the formalism from nearest-neighbor to even longer-range interactions is trivial, so we will not discuss this case explicitly.

[75]D. K. Campbell, J. T. Gammel, and E. Y. Loh, Phys. Rev. B **42**, 475 (1990).

[76]Y. Nomura, M. Kaltak, K. Nakamura, C. Taranto, S. Sakai, A. Toschi, R. Arita, K. Held, G. Kresse, and M. Imada, Phys. Rev. B **86**, 085117 (2012).

[77]L. Vaugier, Ph.D. thesis, Ecole Polytechnique, Palaiseau, France, 2012.

[78]W. Metzner and D. Vollhardt, Phys. Rev. Lett. **62**, 324 (1989).

[79]G. D. Mahan, *Many-Particle Physics*, 2nd. ed (Plenum, New York, NY, 1993).

[80]In this case, one can check that within EDMFT, $\mathcal{U} = U$.

[81]E. Lange, Mod. Phys. Lett. B **12**, 915 (1998).